1521-0103/361/2/312–321$25.00
THE JOURNAL OF PHARMACOLOGY AND EXPERIMENTAL THERAPEUTICS

https://doi.org/10.1124/jpet.116.238022
J Pharmacol Exp Ther 361:312–321, May 2017

Dual Inhibition of Bruton's Tyrosine Kinase and Phosphoinositide-3-Kinase p110δ as a Therapeutic Approach to Treat Non-Hodgkin's B Cell Malignancies[S]

Jennifer Alfaro,[1] Felipe Pérez de Arce, Sebastián Belmar, Glenda Fuentealba, Patricio Avila, Gonzalo Ureta, Camila Flores, Claudia Acuña, Luz Delgado, Diana Gaete, Brahmam Pujala, Anup Barde, Anjan K. Nayak, T. V. R. Upendra, Dhananjay Patel, Shailender Chauhan, Vijay K. Sharma, Stacy Kanno, Ramona G. Almirez, David T. Hung, Sarvajit Chakravarty, Roopa Rai, Sebastián Bernales, Kevin P. Quinn, Son M. Pham, and Emma McCullagh[1]

Translational Research Group, Fundación Ciencia y Vida, Santiago, Chile (J.A., F.P.d.A., S.Bel., G.F., P.A., G.U., C.F., C.A., L.D., D.G.); Biological Sciences Department, Facultad de Ciencias Biológicas, Universidad Andrés Bello, Región de Valparaíso, Chile (F.P.d.A., S.Bel.); Chemistry Group, Integral BioSciences, Pvt. Ltd., Noida, India (B.P., A.B., A.K.N., T.V.R.U., D.P., S.C., V.K.S.); and Discovery Research, Medivation, Inc., now Pfizer, San Francisco, California (S.K., R.G.A., D.T.H., S.C., R.R., S.Ber., K.P.Q., S.M.P., E.M.)

Received September 28, 2016; accepted March 10, 2017

ABSTRACT

Although new targeted therapies, such as ibrutinib and idelalisib, have made a large impact on non-Hodgkin's lymphoma (NHL) patients, the disease is often fatal because patients are initially resistant to these targeted therapies, or because they eventually develop resistance. New drugs and treatments are necessary for these patients. One attractive approach is to inhibit multiple parallel pathways that drive the growth of these hematologic tumors, possibly prolonging the duration of the response and reducing resistance. Early clinical trials have tested this approach by dosing two drugs in combination in NHL patients. We discovered a single molecule, MDVN1003 (1-(5-amino-2,3-dihydro-1H-inden-2-yl)-3-(8-fluoro-3,4-dihydro-2H-benzo[b][1,4]oxazin-6-yl)-1H-pyrazolo[3,4-d]pyrimidin-4-amine), that inhibits Bruton's tyrosine kinase and phosphatidylinositol-3-kinase δ, two proteins regulated by the B cell receptor that drive the growth of many NHLs. In this report, we show that this dual inhibitor prevents the activation of B cells and inhibits the phosphorylation of protein kinase B and extracellular signal-regulated kinase 1/2, two downstream mediators that are important for this process. Additionally, MDVN1003 induces cell death in a B cell lymphoma cell line but not in an irrelevant erythroblast cell line. Importantly, we found that this orally bioavailable dual inhibitor reduced tumor growth in a B cell lymphoma xenograft model more effectively than either ibrutinib or idelalisib. Taken together, these results suggest that dual inhibition of these two key pathways by a single molecule could be a viable approach for treatment of NHL patients.

Introduction

Non-Hodgkin's lymphomas (NHLs) are among the most common of human cancers, and despite advancements of medical treatments and improvements in patient outcomes, the disease has a 30% mortality rate within the first five years after diagnosis (Howlader et al., 2014; Swerdlow et al., 2016). Activation of B cell receptor (BCR) signaling is a significant mechanistic driver of the development and growth of B cell–derived lymphoid tumors (Buchner and Muschen, 2014; Koehrer and Burger, 2016). Basal BCR signaling is necessary for the survival of B cells (Verkoczy et al., 2007; Wang et al., 2013), and signaling through the complex pathway is amplified during B cell activation (Woyach et al., 2012). The BCR is comprised of a membrane immunoglobulin complex, the ligation of which results in the phosphorylation of the cytoplasmic immunoreceptor tyrosine-based activation motif of BCR coreceptors by two kinases, Lyn (Lck/Yes novel tyrosine kinase) and Syk (spleen tyrosine kinase). Propagation of the signal occurs via several parallel and interconnected pathways. Two important

Financial support for this research was provided by Medivation, Inc., now Pfizer. Some authors are employees of Medivation, now Pfizer. Some authors are inventors on patents related to the subject matter.
[1]J.A. and E.M. contributed equally to this work.
https://doi.org/10.1124/jpet.116.238022.
[S] This article has supplemental material available at jpet.aspetjournals.org.

ABBREVIATIONS: AKT, protein kinase B; BCR, B cell receptor; BTK, Bruton's tyrosine kinase; CLL, chronic lymphocytic leukemia; ERK 1/2, extracellular signal-regulated kinase 1/2; MCL, mantle cell lymphoma; MDVN1001, 5-(8-fluoro-3,4-dihydro-2H-benzo[b][1,4]oxazin-6-yl)-7-(5-(piperidin-4-yl)-2,3-dihydro-1H-inden-2-yl)-7H-pyrrolo[2,3-d]pyrimidin-4-amine; MDVN1002, 1-(5-amino-2,3-dihydro-1H-inden-2-yl)-3-(3-fluoro-4-isopropoxyphenyl)-1H-pyrazolo[3,4-d]pyrimidin-4-amine; MDVN1003, 1-(5-amino-2,3-dihydro-1H-inden-2-yl)-3-(8-fluoro-3,4-dihydro-2H-benzo[b][1,4]oxazin-6-yl)-1H-pyrazolo[3,4-d]pyrimidin-4-amine; NHL, non-Hodgkin's lymphoma; pAKT, phosphorylated AKT; PCI-29732, 1-Cyclopentyl-3-(4-phenoxyphenyl)-1H-pyrazolo[3,4-d]pyrimidin-4-amine; pErk, phosphorylated Erk; PI3Kδ, phosphatidylinositol-3-kinase δ; PK, pharmacokinetic; SW13, 2-((4-amino-3-(3-fluoro-5-hydroxyphenyl)-1H-pyrazolo[3,4-d]pyrimidin-1-yl)methyl)-5-methyl-3-(o-tolyl)quinazolin-4(3H)-one.

kinases downstream of the BCR are Bruton's tyrosine kinase (BTK) and phosphatidylinositol-3-kinase δ (PI3Kδ) (Seda and Mraz, 2015).

BTK is a member of the Tec family of tyrosine kinases and is recruited to the cell membrane after the activation of the BCR. Together with Syk, BTK phosphorylates phospholipase C-γ2, producing the classic second messengers diacylglycerol and inositol-1,4,5-triphosphate from phosphatidylinositol-4,5-bisphosphate. Diacylglycerol activates protein kinase C, and inositol-1,4,5-triphosphate triggers the release of intracellular calcium, resulting in the activation of several downstream signaling molecules, including extracellular signal-regulated kinase 1/2 (ERK 1/2) (Tomlinson et al., 2001). PI3Kδ is also recruited to the cell membrane and activated in response to BCR signaling. PI3K is a heterodimer composed of the p85 regulatory subunit and the p110 catalytic subunit, which in B cells is the δ isoform. PI3Kδ is involved in recruiting BTK to the cell membrane and phosphorylates and activates several downstream signaling molecules, including protein kinase B (AKT) (Fruman and Rommel, 2014). The BTK and PI3Kδ signaling pathways are not insulated from one another, and there is evidence of cross-talk between them (Puri et al., 2013). Both BTK and PI3Kδ are involved in normal B cell signal propagation but have been identified as being aberrantly activated in many B cell malignancies (Seda and Mraz, 2015). These proteins are the targets of the approved therapies: ibrutinib, an irreversible BTK inhibitor, and idelalisib, a reversible PI3Kδ inhibitor.

Ibrutinib blocks the enzymatic activity of BTK through covalent binding to a conserved cysteine residue (Cys481) in the active site (Honigberg et al., 2010). Ibrutinib was approved by the Food and Drug Administration for use in mantle cell lymphoma (MCL), chronic lymphocytic leukemia (CLL), and Waldenström's macroglobulinemia patients. Idelalisib is a highly selective ATP competitive inhibitor of PI3Kδ (Lannutti et al., 2011; Marini et al., 2016) and has been approved for use in CLL, follicular cell NHL, and relapsed small lymphocytic lymphoma patients (Do et al., 2016).

Although the approval of these targeted therapies by the Food and Drug Administration was a significant advance, it has been reported that about 30% of MCL and CLL patients show primary resistance to ibrutinib (Tucker and Rule, 2015). Furthermore, a subset of patients who initially respond to and receive prolonged treatment of ibrutinib eventually relapse due to the development of mutations in BTK that prevent the covalent binding of ibrutinib or gain-of-function mutations in phospholipase C-γ2 (Byrd et al., 2013; Wang et al., 2013; Smith, 2015). The resistance to idelalisib is not as well understood. Several reports have suggested that combination dosing of ibrutinib and idelalisib could be advantageous since targeting parallel pathways downstream of the BCR could reduce the risk of signal switching, leading to escape from tumor growth inhibition (Jones and Byrd, 2014; Mathews Griner et al., 2014; Zhang et al., 2014; de Rooij et al., 2015; Koehrer and Burger, 2016).

In this report, we describe proof-of-concept preclinical studies with tool compound MDVN1003 (1-(5-amino-2,3-dihydro-1H-inden-2-yl)-3-(8-fluoro-3,4-dihydro-2H-benzo[b][1,4]oxazin-6-yl)-1H-pyrazolo[3,4-d]pyrimidin-4-amine), a first-in-class dual inhibitor of BTK and PI3Kδ kinases (Pujala et al., 2016). We found that MDVN1003 inhibits B cell activation upon BCR cross-linking ex vivo and in vivo, a phenomenon dependent on BTK and PI3Kδ. Additionally, MDVN1003 induces apoptosis and decreases viability of DOHH-2 cells, an NHL cell line. Finally, MDVN1003, an orally bioavailable molecule in mice, rats, and dogs, showed significant antitumor effects in an NHL xenograft model in mice. This effect was similar to that seen with combination dosing of ibrutinib and idelalisib in the same model and greater than each of these drugs dosed as single agents. Our results suggest that a dual inhibitor of BTK and PI3Kδ could be an effective treatment strategy for B cell lymphoma patients.

Materials and Methods

Reagents and Tumor Cell Lines. Ibrutinib (CAS 936563-96-1) and idelalisib (CAS 870281-82-6) were purchased from ChemShuttle (Union City, CA). Compounds MDVN1003, MDVN1001 (5-(8-fluoro-3,4-dihydro-2H-benzo[b][1,4]oxazin-6-yl)-7-(5-(piperidin-4-yl)-2,3-dihydro-1H-inden-2-yl)-7H-pyrrolo[2,3-d]pyrimidin-4-amine), and MDVN1002 (1-(5-amino-2,3-dihydro-1H-inden-2-yl)-3-(3-fluoro-4-isopropoxyphenyl)-1H-pyrazolo[3,4-d]pyrimidin-4-amine) were synthesized at Integral BioSciences, Pvt. Ltd. (Noida, India). All tumor cell lines were purchased from the American Type Culture Collection (Manassas, VA) and were tested for mycoplasma by polymerase chain reaction. All revived cells were used within 20 passages and cultured for less than 6 months. Ramos and DOHH-2 cells were maintained in RPMI 1640 medium containing 10% heat-inactivated fetal bovine serum supplemented with penicillin and streptomycin.

Enzymatic Kinase Assays. In vitro kinase activity assays were performed by Reaction Biology Corporation (www.reactionbiology.com) as described on the Web site and as described previously (Pujala et al., 2016).

Assessment of BCR-Dependent Signaling Levels. Ramos cells were pretreated for 30 minutes with compounds (0.1 or 1 μM final concentration) and then stimulated with α-human IgM (1.3 μg/ml) (#109-006-129; Jackson ImmunoResearch Laboratories, Inc., Westgrove, PA) for 5 minutes. Levels of phosphorylated AKT (pAKT) (#4060; Cell Signaling Technology, Danvers, MA), AKT (#9272; Cell SignalingTechnology), phosphorylated Erk (pErk; T202, Y204) (#4377; Cell Signaling Technology), and ERK (#4396; Cell Signaling Technology) were detected by western blot using the ChemiDoc Imaging System (Bio-Rad, Hercules, CA).

Measuring B Cell Activation by CD69 Expression. Splenocytes (1×10^6 cells/well) were seeded in a 24-well plate and pretreated for 30 minutes with compounds at indicated concentrations and then activated for 4 hours with α-mouse IgD (3 μg/ml) (YULLOMD6-05; Accurate Chemical, Westbury, NY). Cells were stained with α-B220 PE (#553090; BD Biosciences, San Jose, CA), α-CD69 APC (#130-103-947; Miltenyi Biotec, Gladbach, Germany), and with a live/dead fixable aqua dead cell kit (#L34957; ThermoFisher Scientific, Grand Island, NY) and analyzed by flow cytometry using a MACSQuant Analyzer 10 flow cytometer (Miltenyi Biotech, Gladbach, Germany). At each concentration of compound tested, the inhibition of B cell activation was calculated as the percentage of live B cells expressing CD69 in the presence of the compound divided by the percentage of live B cells expressing CD69 in the vehicle control. Splenocytes from three individual mice were treated independently per condition tested. The IC_{50} was calculated from the average of the three independent experiments, and curve fitting was done by nonlinear regression using GraphPad Prism (GraphPad Software, La Jolla, CA).

Viability Assay. DOHH-2 or HEL 92.1.7 cells were seeded in a 96-well white plate overnight at a density of 5000 cells/well. Cells were treated with compounds at the indicated concentrations for 72 hours. Cell viability was measured using a Cell Titer-glo kit (Promega, Madison, WI) as described by the manufacturer. The IC_{50} was calculated from the curve fitted to the data points by nonlinear regression using GraphPad Prism.

Apoptosis Assay. DOHH-2 cells were seeded in a 24-well plate at 0.5×10^6 cells/well. Cells were then treated with compounds at 1 μM for 4 hours, and apoptosis was measured by flow cytometry (MACSQuant Analyzer 10) using an Annexin V FITC apoptosis detection kit (#556547; BD Biosciences).

Pharmacokinetic Analysis. All animal studies were done as per protocols approved by the Institutional Animal Care and Use Committee at Medivation or its subsidiaries. See Supplemental Material for experimental details of mouse, rat, and dog pharmacokinetic (PK) studies.

Measuring B Cell Activation by CD69 Expression In Vivo. BALB/c mice were orally dosed with compounds ($n = 3$ per group) at indicated concentrations for 30 minutes, and then mice were injected intravenously in the tail vein with 100 μg of α-IgD (YULLOMD6-05; Accurate Chemical, Westbury, NY) for 5 hours. Splenocytes were isolated and stained and analyzed as described earlier. The percentage of live B cells that express CD69 from mice treated with α-IgD and compound was normalized to the percentage of live B cells that express CD69 from mice treated with α-IgD alone.

Mouse Xenograft Model. All animal studies were done as per protocols approved by the Institutional Animal Care and Use Committee at Medivation or its subsidiaries.

DOHH-2 cells were maintained in RPMI 1640 medium supplemented with 10% fetal bovine serum and were passaged twice weekly. While in the exponential growth phase, 5 million DOHH-2 cells in 0.1 ml of phosphate-buffered saline (1:1 ratio with matrigel) were inoculated into the right flanks of 6- to 7-week-old female CB17/SCID mice (denoted as day 0). When the average tumor volume reached 118 mm^3, mice were randomly grouped into eight groups ($n = 10$ per group). Tumor volume and body weight were measured twice a week. The experiment was terminated when the average tumor volume of the vehicle group reached >2000 mm^3, and plasma and tumor samples were collected from each mouse ($n = 3$ mice per group were sacrificed 5 minutes before the final dose, $n = 3$ mice per group were sacrificed 30 minutes post final dose, and $n = 4$ mice per group were sacrificed 6 hours post final dose). Statistical analysis (Kruskal-Wallis corrected for multiple comparisons) was done on the tumor volumes of the groups over time.

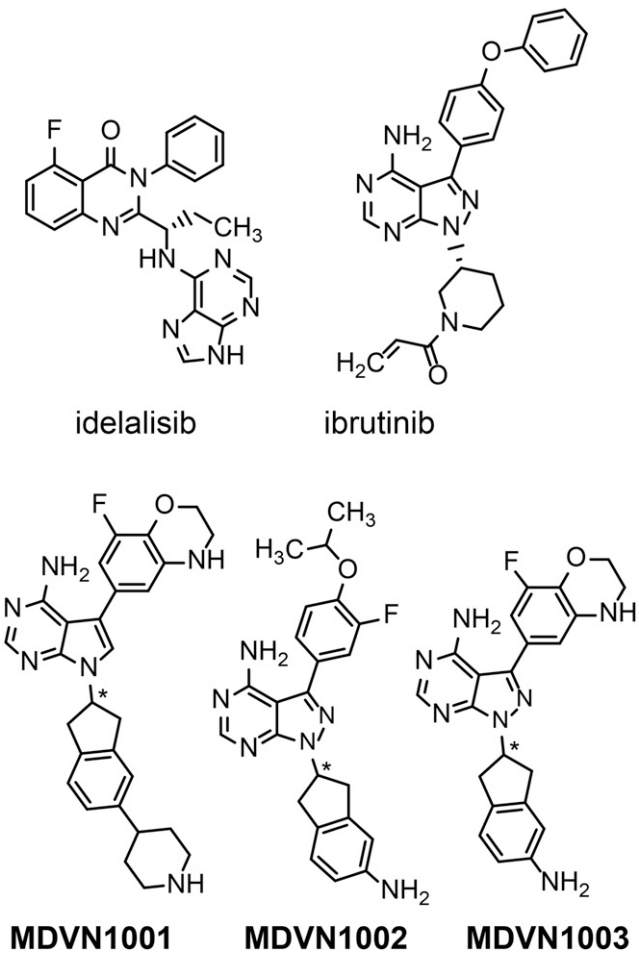

Fig. 1. Novel reversible inhibitors of PI3Kd or BTK. The structures of idelalisib, ibrutinib, and three novel compounds (MDVN1001, MDVN1002, and MDVN1003) are detailed. MDVN1001, MDVN1002, and MDVN1003 are enantiomerically pure, but the absolute configuration has yet to be determined (asterisks in the structures mark the stereogenic centers).

Results

As described (Pujala et al., 2016), we aimed to discover reversible dual BTK and PI3Kδ inhibitors based on the similarities between a reversible BTK inhibitor, PCI-29732 (1-Cyclopentyl-3-(4-phenoxyphenyl)-1H-pyrazolo[3,4-d]pyrimidin-4-amine) (Pan et al., 2007; Marcotte et al., 2010), and a PI3Kδ/γ dual inhibitor, SW13 (2-((4-amino-3-(3-fluoro-5-hydroxyphenyl)-1H-pyrazolo[3,4-d]pyrimidin-1-yl)methyl)-5-methyl-3-(o-tolyl)quinazolin-4(3H)-one) (Berndt et al., 2010). We identified three compounds (Fig. 1), two of which are more potent against one of the two receptors and one compound that is a more potent dual inhibitor (Table 1; synthesis in Supplemental Methods). On the one hand, MDVN1001 is a potent BTK inhibitor (IC_{50} 0.9 nM) and a relatively weak PI3Kδ inhibitor (IC_{50} 149 nM). On the other hand, MDVN1002 strongly inhibited PI3Kδ (IC_{50} 25.9 nM) more than it did BTK (IC_{50} 695 nM). However, the dual inhibitor, MDVN1003, potently inhibited both kinases (BTK with an IC_{50} of 32.3 nM, and PI3Kδ with an IC_{50} of 16.9 nM). As expected, the control compounds, idelalisib and ibrutinib, inhibited one kinase more strongly than the other. Idelalisib, an ATP competitive, reversible inhibitor of PI3Kδ, inhibited PI3Kδ with an IC_{50} of 1.2 nM, whereas it did not measurably inhibit BTK at any concentration tested. Ibrutinib, an irreversible inhibitor of BTK, potently inhibited BTK (IC_{50} 0.142 nM) and weakly inhibited PI3Kδ (IC_{50} 640 nM).

To investigate the effects of these molecules on signaling through the BCR pathway, phosphorylation of ERK 1/2 and AKT was measured in the Ramos Burkitt's B cell lymphoma cell line. Ramos cells were pretreated with vehicle or 0.1 μM idelalisib, ibrutinib, MDVN1001, MDVN1002, MDVN1003, or an equimolar cotreatment of idelalisib and ibrutinib (subsequently referred to as "combo"). Cells were treated with α-human IgM for 5 minutes to cross-link and activate the BCR. Levels of phosphorylated ERK 1/2 and AKT were detected by western blot (Fig. 2). Treatment with α-human IgM increased the levels of phosphorylated AKT and ERK 1/2 as compared with the vehicle alone, indicating the BCR signaling pathway was activated (Fig. 2, lanes 1 and 2). Ibrutinib and idelalisib treatments significantly reduced the levels of pERK 1/2 and pAKT. Neither MDVN1001 nor MDVN1002 significantly affected levels of pAKT or pERK 1/2 when tested at 0.1 μM. However, these compounds did inhibit the phosphorylation of AKT and ERK 1/2 at higher concentrations (Supplemental Fig. 1). Combination treatment of idelalisib and ibrutinib potently inhibited levels of both pAKT and pERK 1/2 (Fig. 2). The MDVN1001 and MDVN1002 combination treatment (combo MDVN) also inhibited the

TABLE 1
IC_{50} values for compounds against PI3Kδ and BTK in kinase inhibition assay

	PI3Kδ	BTK
	nM	*nM*
Idelalisib	1.2	>100,000
Ibrutinib	640	0.142
MDVN1001	149	0.9
MDVN1002	25.9	695
MDVN1003	16.9	32.3

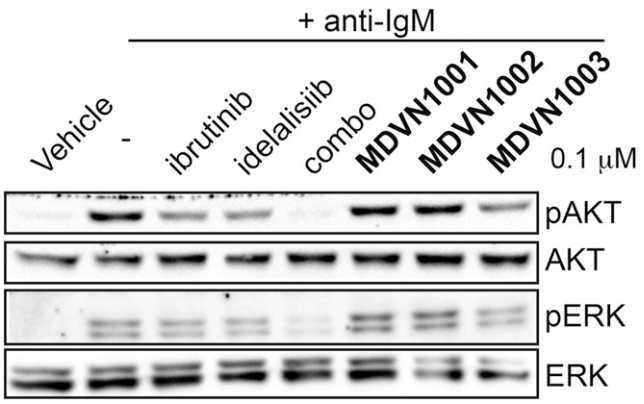

Fig. 2. BTK and PI3Kδ inhibitor compounds differentially inhibit the phosphorylation of downstream signaling molecules ATK and ERK. Ramos cells were pretreated for 30 minutes with either dimethylsulfoxide (lanes labeled vehicle and -) or the indicated compounds... the indicated compounds (0.1 μM). All samples, except for the vehicle control, were treated with α-IgM (1.3 μg/ml) for 5 minutes to activate BCR signaling. Levels of pAKT and pERK 1/2 and the corresponding total proteins were determined by western blot. Combo is equimolar (0.1 μM) treatment of ibrutinib and idelalisib.

phosphorylation of AKT and ERK1/2, although not as potently as the combination treatment of the two approved inhibitors (Supplemental Fig. 1). Treatment with the dual BTK/PI3Kδ inhibitor compound MDVN1003 inhibited the phosphorylation of AKT and ERK 1/2 at both the low concentration (0.1 μM) and the high concentration (1 μM) and did so more potently than the combination of MDVN1001 and MDVN1002 (Fig. 2; Supplemental Fig. 1). Taken together, these data show that MDVN1003 is a more potent inhibitor of BCR signaling than either MDVN1001 or MDVN1002 dosed individually or in combination and suggest that the dual inhibition of BTK and PI3Kδ may have a synergistic effect on downstream signaling molecules.

We wanted to further investigate the potential synergy of inhibiting both BTK and PI3Kδ in B cell lymphomas using ibrutinib, idelalisib, and MDVN1003 as tool compounds. These compounds provided us with the necessary tools to study treatment with monotherapies and dual inhibition. MDVN1003 is more potent than either MDVN1001 or MDVN1002 (or the combination of both) in the cell-based assay and allowed us to study dual inhibition in a single molecule.

To understand the selectivity profile of MDVN1003 and how it compares to those of ibrutinib and idelalisib, we tested these compounds in a kinase panel at 1 μM. Idelalisib is a highly selective PI3Kδ inhibitor and inhibited four other kinases (out of 374 tested) greater than 50%. Ibrutinib inhibited 34 kinases (out of 374 tested) more than 50% (Fig. 3). MDVN1003 behaved similarly to ibrutinib in the kinase panel and inhibited 50 kinases (out of 402 tested) at greater than 50%, with a preference for tyrosine kinases (Fig. 3). Among the kinases most potently inhibited by MDVN1003 were BTK, PI3Kδ, and the related Tec- and PI3K-family kinases (Fig. 3; Table 2).

We next investigated the effects of MDVN1003 on the activation of primary B cells ex vivo. Mouse splenocytes were pretreated with ibrutinib, idelalisib, combo, or MDVN1003 for 30 minutes. Cells were treated with α-IgD for 4 hours to activate B cells. Anti-IgD cross-links the surface immunoglobulin and activates the B cell, which upregulates the early B cell activation marker CD69 (Sancho et al., 2005). Activated B cells were detected by flow cytometry as B22+CD69+ in a gate of live cells. The inhibition of B cell activation was measured by the percentage of live B cells that expressed CD69 on the cell surface in treated samples as compared with the α-IgD control. Ibrutinib and idelalisib potently inhibited B cell activation, with IC_{50} values of 6.9 and 5.4 nM, respectively (Fig. 4A; Table 3). Idelalisib, but not ibrutinib, produced full inhibition of B cell activation. The combo treatment of both compounds showed a modest additive effect with an IC_{50} of 1.1 nM (Fig. 4A; Table 3) and produced full inhibition of B cell activation. MDVN1003 inhibited B cell activation with an IC_{50} of 25.2 nM (Fig. 4A; Table 3). Although less potent, MDVN1003 was equally as efficacious as idelalisib and the combo treatment and fully inhibited B cell activation.

Signaling through the BCR is often a driver of tumor growth in B cell malignancies (Buchner and Muschen, 2014), and it has been reported that both ibrutinib and idelalisib reduce cell viability and induce apoptosis in NHL B cell lines (Honigberg et al., 2007; Lannutti et al., 2011; Qu et al., 2015). To determine whether MDVN1003 behaved similarly to the approved drugs, we measured the effect of MDVN1003 on the viability of DOHH-2 cells, a non-Hodgkin's B cell lymphoma line that expresses BTK and PI3Kδ. After 72 hours of treatment, MDVN1003 effectively killed DOHH-2 cells with an IC_{50} of 1.34 μM, whereas the IC_{50} values for ibrutinib and idelalisib were 0.023 and 0.86 μM, respectively (Fig. 4B; Table 3). The IC_{50} for the combo treatment was 0.0084 μM, suggesting an additive effect on cell viability in inhibiting both BTK and PI3Kδ. The cytotoxicity induced by these compounds was determined to be apoptosis, as indicated by the significant population of Annexin V+ propidium iodide− cells in treatment groups as compared with the vehicle control ($P < 0.0001$, one-way analysis of variance) (Fig. 4C). Combination treatment of MDVN1001, the BTK inhibitor, and MDVN1002, the PI3Kδ inhibitor, also showed an additive effect on cell viability of DOHH-2 cells with an IC_{50} of 0.87 μM, as compared with IC_{50} values of 1.47 μM with MDVN1001 alone and 2.75 μM with MDVN1002 alone (Supplemental Fig. 2). Although a modest effect, these data suggest a benefit of dual inhibition of BTK and PI3Kδ.

To understand if the cytotoxicity of these compounds was dependent on inhibition of BTK and PI3Kδ, we tested the effects of the compounds on viability of HEL 92.1.7 erythroblast-like cells that do not express these kinases. The IC_{50} values of ibrutinib, idelalisib, combo, and MDVN1003 were all greater than 10 μM (Table 3), suggesting that these compounds are preferentially cytotoxic in cells that express BTK and PI3Kδ.

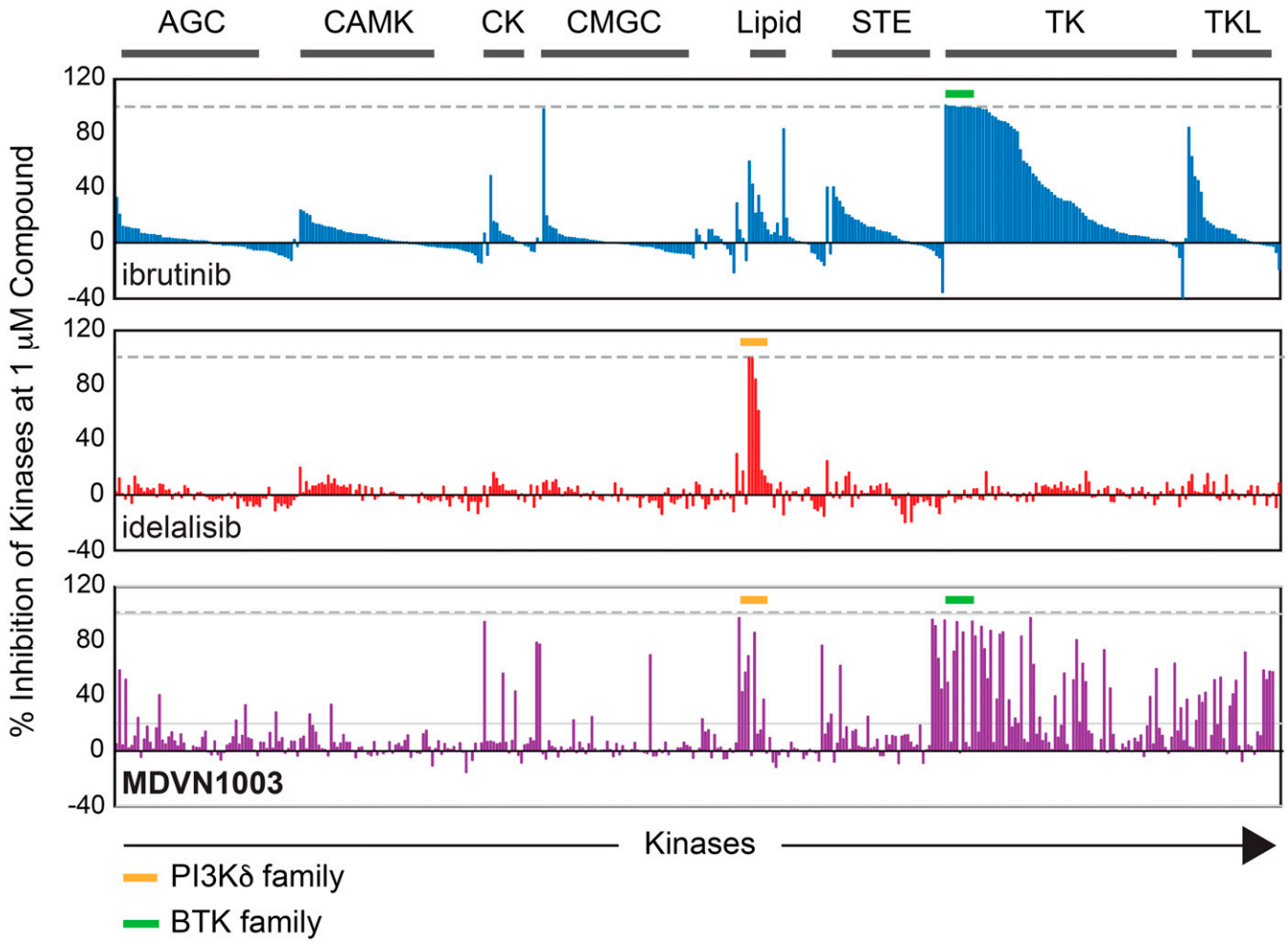

Fig. 3. The kinase profile of MDVN1003 is similar to that of ibrutinib. Ibrutinib, idelalisib, and MDVN1003 were tested at 1 μM against >350 kinases in enzymatic assays. The percentage of inhibition is plotted for each kinase. The values for ibrutinib are shown in blue in the top panel, the values for idelalisib are shown in red in the middle panel, and the values for MDVN1003 are shown in purple in the bottom panel. The kinases are organized by family as indicated above the graphs. The PI3Kδ family of kinases are highlighted by the orange line, and the BTK family are highlighted by the green line. AGC, AGC Kinase Group; CAMK, Ca2+/calmodulin-dependent protein kinase family; CK, Casein kinase 1 family; CMGC, CMGC kinase family; Lipid, Lipid Kinase family; STE, STE kinase family; TK, Tyrosine Kinase family; TKL, Tyrosine Kinase-Like family.

To study the pharmacology of MDVN1003 in vivo, we investigated the PK properties of this molecule across species. The PK profiles of MDVN1003 in mice, rats, and dogs after a single oral dose are shown in Fig. 5. The noncompartmental analysis PK parameters of MDVN1003 in mice, rats, and dogs are summarized in Table 4. Following oral administration in mice, MDVN1003 showed rapid absorption, with a time of maximum concentration in plasma (t_{max}) of 0.25 hours, and then declined with a biexponential decay and an elimination half-life ($t_{1/2}$) of 1.3 hours (Fig. 5). The absolute oral bioavailability (F) was acceptable at 40%. Following intravenous administration in mice, MDVN1003 showed low systemic clearance (0.6 l/h/kg) that was 13% of hepatic blood flow in the mouse [Q_H = 4.7 l/h/kg (Davies and Morris, 1993)] and a moderate volume of distribution (V_d = 3.4 l/kg), as shown in Table 4. Following oral administration in rats, MDVN1003 showed rapid absorption with a t_{max} of 0.25 hours, and then declined with a biexponential decay and a $t_{1/2}$ of 1.2 hours (Fig. 5). The absolute oral bioavailability (F) was an acceptable 31%. Following intravenous administration in rats, MDVN1003 showed high systemic clearance (4.94 l/h/kg) that was 150% of hepatic blood flow in the rat [Q_H = 3.31 l/h/kg (Davies and Morris, 1993)] and a moderate volume of distribution (V_d = 2.0 l/kg), as shown in Table 4. Following oral administration in dog, MDVN1003 showed rapid absorption, with a t_{max} of 0.42 hours, and then declined with a biexponential

TABLE 2
IC_{50} values for compounds against BTK and PI3Kδ kinase family members

	Idelalisib	Ibrutinib	MDVN1003
	nM	*nM*	*nM*
PI3Kα	354	>100,000	275
PI3Kβ	90.2	>100,000	708
PI3Kγ	30	>1000	107
BMX/ETK	>100,000	<0.1	44.5
ITK	>100,000	19.3	>300
TEC	>100,000	<0.1	211

BMX/ETK, epithelial and endothelial tyrosine kinase; ITK, interleukin-2–inducible T-cell kinase dimethyl sulfoxide; TEC, Tec protein tyrosine kinase.

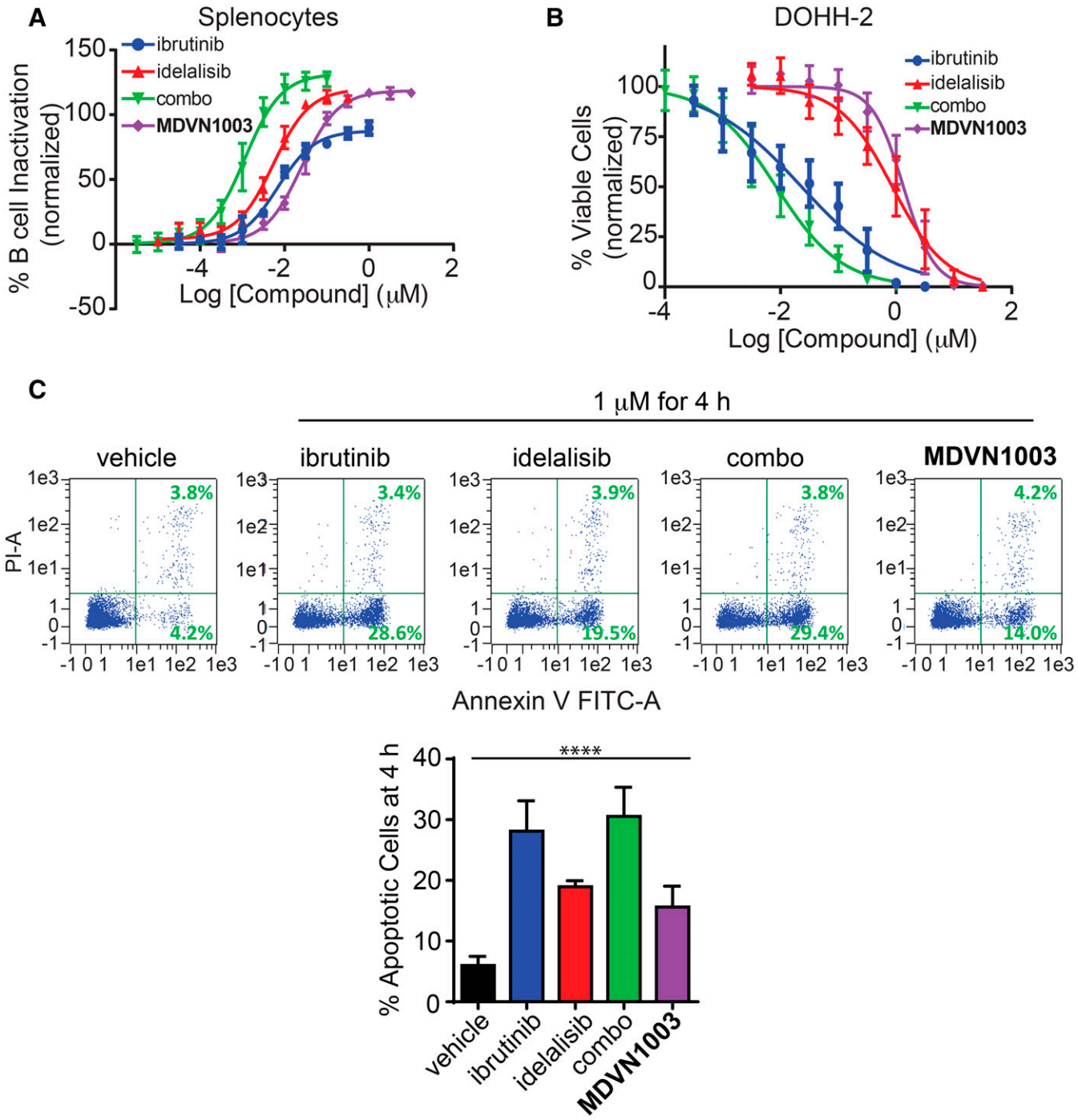

Fig. 4. MDVN1003 inhibits B cell activation in mouse splenocytes and induces apoptosis in DOHH-2 B cell lymphoma cells. (A) Splenocytes were pretreated with the indicated compounds at different concentrations for 30 minutes and then treated with α-IgD (3 μg/ml) for 4 hours to activate BCR signaling. Activated B cells were identified by flow cytometry as the B220+CD69+ cells in a live gate. To calculate the effect of each compound on the inhibition of B cell activation, the percentage of B220+CD69+ cells in each condition was normalized to the α-IgD vehicle control. The IC_{50} was calculated from the curve fitted to the data points by nonlinear regression using GraphPad Prism. (B) DOHH-2 cells were treated with compounds at the indicated concentrations for 72 hours. Cell viability was measured as described in the *Materials and Methods*. The IC_{50} was calculated from the curve fitted to the data points by nonlinear regression using GraphPad Prism. (C) DOHH-2 cells were treated with compounds at 1 μM for 4 hours, and apoptosis was measured by flow cytometry using an Annexin V FITC apoptosis detection kit. Apoptotic cells were determined as Annexin V+ propidium iodide (PI)− by flow cytometry. Dot plots from a representative experiment are shown in the top panels, and a summary of the percentages of apoptotic cells from four independent experiments is plotted in the bottom panel (mean ± standard deviation, ****$P < 0.0001$, one-way analysis of variance). PI-A, propidium idodide area.

decay and a $t_{1/2}$ of 1.5 hours (Fig. 5). The absolute oral bioavailability (F) was a moderately high 62%. Following intravenous administration in dog, MDVN1003 showed moderate systemic clearance (1.23 l/h/kg) that was 66% of hepatic blood flow in the dog [Q_H = 1.85 l/h/kg (Davies and Morris, 1993)] and a moderate volume of distribution (V_d = 1.0 l/kg), as shown in Table 4.

Given the low clearance and acceptable oral bioavailability of MDVN1003 in mice, we aimed to show pharmacological

efficacy, as proof of concept, in two in vivo mouse models: a model of B cell activation and a xenograft model of non-Hodgkin's B cell lymphoma. To test the effect of the compounds on B cell activation in vivo, BALB/c mice were prophylactically dosed with different oral doses of compound for 30 minutes prior to being challenged with an α-IgD antibody administered intravenously via tail vein to activate BCR signaling for up to 5 hours (Fig. 6A). After the treatment, splenocytes were isolated, and activated B cells were detected by flow cytometry as B220+CD69+ in a gate of live cells. With no α-IgD treatment, between 3 and 5% of B cells were active basally (CD69+) in spleens (data not shown). In mice treated orally with vehicle and intravenously with α-IgD, around 30% of B cells were CD69+ (data not shown). This value was set to 100% activation, and the percentages of CD69+ B cells in the drug-treated mice were normalized to the percentage of CD69+ B cells in the α-IgD–treated control group. Ibrutinib effectively inhibited (>50%) B cell activation at all doses tested (10, 50, and 100 mg/kg), whereas idelalisib only inhibited B cell activation by 50% at 10 mg/kg (Fig. 6B) but was effective at higher doses. MDVN1003 did not inhibit B cell activation at 10 mg/kg but inhibited activation by 75% at 50 and 100 mg/kg (Fig. 6B). The lack of a dose response at 50 and 100 mg/kg of MDVN1003 may suggest that absorption of this compound is already saturated at 50 mg/kg.

Given that MDVN1003 induced cell death in DOHH-2 cells and inhibited B cell activation in vivo, we tested whether this compound was able to inhibit tumor growth in vivo in a DOHH-2 B cell lymphoma xenograft model. Six- to 7-week-old CB17/SCID mice were inoculated in the right flank with 5×10^6 DOHH-2 cells. Mice were grouped ($n = 10$/group) and dosing began when tumors reached an average of 100 mm^3. Dosing was terminated when the average tumor volume of the vehicle group reached 2000 mm^3. Mice were placed into one of eight groups and dosed with vehicle, two doses of ibrutinib (15 or 30 mg/kg), two doses of idelalisib (25 or 50 mg/kg), two combinations of ibrutinib and idelalisib (15 mg/kg ibrutinib/25 mg/kg idelalisib or 30 mg/kg ibrutinib/50 mg/kg idelalisib), or one dose level of MDVN1003 (100 mg/kg). Ibrutinib was dosed once daily due to its irreversible binding, and idelalisib and MDVN1003 were both dosed twice daily. Mice were monitored for body weight and tumor volume over the 21 days of dosing. The body weight of the mice was unaffected by the treatments (Fig. 6C). Tumor growth was slowed by combination treatment of ibrutinib and idelalisib and by treatment with MDVN1003 (Fig. 6, D and E). On the final day of dosing (day 31 postinoculation), ibrutinib at either 15 or 30 mg/kg reduced average tumor volume by 15.7 and 24.7%, respectively, and idelalisib at 25 or 50 mg/kg reduced average tumor volume by 6.6 and 14.2%, respectively, as compared with the vehicle control group (not statistically significant). When dosed in combination, the average tumor volume of the ibrutinib (15 mg/kg) and idelalisib (25 mg/kg) low combo group was reduced by 38.1% as compared with the vehicle group, whereas tumors in the ibrutinib (30 mg/kg) and idelalisib (50 mg/kg) high combo group were reduced by 57.9% on average as compared with the vehicle control group ($P < 0.001$, Kruskal-Wallis corrected for multiple comparisons). Treatment with MDVN1003 reduced tumor growth by 45.2% ($P < 0.01$, Kruskal-Wallis corrected for multiple comparisons).

TABLE 3

IC_{50} values for the inhibition of B cell activation in primary mouse splenocytes and cytotoxic effects in DOHH-2 lymphoma and HEL 92.1.7 cells

	Primary B Cell Activation (CD69)	DOHH-2 Cell Viability	HEL 92.1.7 Cell Viability
	nM	*nM*	*nM*
Ibrutinib	6.9	23	>10,000
Idelalisib	5.4	860	>10,000
Combo	1.1	8.4	>10,000
MDVN1003	25.2	1340	>10,000

Discussion

The potential advantage of dual inhibition of BTK and PI3Kδ for treatment of NHL lies in the possibility of treating refractory patients or overcoming developed resistance to either BTK or PI3Kδ single inhibitors due to the synergistic or additive effects of blocking two BCR pathway targets. Codosing BTK and PI3Kδ single inhibitors is one approach to gaining the advantage of dual inhibition. Preclinical evidence supports the notion that inhibiting these two pathways could result in synergistic or additive effects. Combination treatments of JeKo1 cells, an MCL cell line, with ibrutinib and idelalisib resulted in decreased adhesion to fibronectin, a BCR-dependent process, as compared with cells treated with each drug individually (de Rooij et al., 2015). The authors found a strong synergistic effect with the dual treatment. In another example, combination treatment of BCWM.1 Waldenström's macroglobulinemia cells with both ibrutinib and the highly selective second-generation PI3Kδ inhibitor TGR-1202 (2-[(1S)-1-[4-amino-3-(3-fluoro-4-propan-2-yloxyphenyl)pyrazolo[3,4-d]pyrimidin-1-yl]ethyl]-6-fluoro-3-(3-fluorophenyl)chromen-4-one TG Therapeutics, New York, NY) resulted in increased cell death as compared with treatment with the individual drugs (Davids et al., 2016).

In this report, we corroborate the findings that cotreatment of B cells with ibrutinib and idelalisib results in effects superior to those seen with either drug dosed individually.

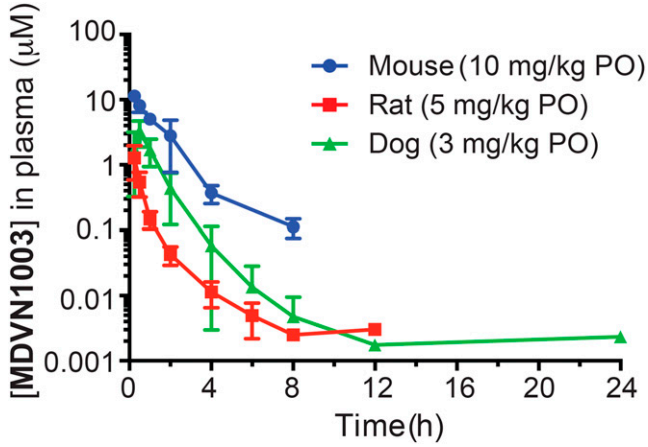

Fig. 5. MDVN1003 concentration-time profile following an oral dose in mouse, rat, and dog. Mice, rats, and dogs were treated orally (PO) or intravenously (data not plotted), and drug concentrations in plasma were monitored over time by liquid chromatography with tandem mass spectrometry analysis. The PK parameters are shown in Table 4.

TABLE 4
Pharmacokinetic parameters of MDVN1003 across species

	Intravenous			Oral		
	Mouse (2 mg/kg)	Rat (2 mg/kg)	Dog (1 mg/kg)	Mouse (10 mg/kg)	Rat (5 mg/kg)	Dog (3 mg/kg)
C_{max} (μM)	5.57 ± 1.66	3.53 ± 0.037	3.34 ± 0.244	11.3 ± 1.29	1.27 ± 0.686	3.32 ± 1.42
AUC_{last} (μM*h)	7.63 ± 0.59	0.968 ± 0.0122	2.04 ± 0.571	15.2 ± 1.87	0.751 ± 0.274	3.77 ± 1.66
Terminal $t_{1/2}$ (h)	7.16 (N = 2)	0.285 ± 0.149	0.62 ± 0.27	1.26	1.17 ± 0.464	1.48 ± 1.26
CL (l/h/kg)	0.594 ± NA	4.94 ± 0.065	1.23 ± 0.327			
V_d (l/kg)	3.445 ± NA	2.02 ± 1.044	1.02 ± 0.153			
t_{max} (h)				0.25	0.25	0.417 ± 0.144
Bioavailability (%)				39.8 ± 4.71	31 ± 11.3	61.7 ± 32.1

AUC_{last}, area under the plasma concentration-time curve up to the last nonzero concentration; CL, systemic clearance; NA, Not Applicable.

The phosphorylation of downstream signaling molecules AKT and ERK 1/2 was significantly dampened in cells treated with both drugs as compared with each drug individually (Fig. 3). Similarly, in the xenograft model, codosing the two inhibitors more effectively reduced the tumor burden than dosing each compound separately (Fig. 6). These data support the hypothesis that targeting two BCR-controlled pathways could be more efficacious than treatment with a monotherapy.

Preclinical data suggesting the potential synergism of inhibiting both BTK and PI3Kδ have spurred clinical trials of combination treatments. TG Therapeutics has several ongoing clinical studies with TGR-1202 and ibrutinib for B cell malignancies, including relapsed or refractory CLL and MCL. From their phase I/Ib study, TG Therapeutics has reported interim results showing an overall response rate of 82% in CLL and 60% in MCL, but has yet to show a reduction in the rate of resistance (Davids et al., 2016).

Although combination treatment of two separate BTK and PI3Kδ inhibitors does provide the advantage of being able to independently control the dose of each inhibitor, we tested the hypothesis that a dual inhibitor in a single molecule could be a potential therapeutic approach for NHL. Having the dual inhibition activity built into a single molecule could ease the toxicology profile since there would be a single set of off-target effects. The cost of treatment of patients may also be lower with a single molecule due to lower manufacturing and formulation costs (Shanafelt et al., 2015). We have previously described our discovery of dual BTK and PI3Kδ inhibitors (Pujala et al., 2016), and here, we report that one of these dual inhibitors does exhibit properties similar to combination dosing of ibrutinib and idelalisib, albeit not as potent or selective.

MDVN1003, although a dual inhibitor of BTK and PI3Kδ, is not as potent an inhibitor as idelalisib and ibrutinib are against their primary targets as measured in in vitro enzymatic assays (Table 1). Despite the difference in potencies, MDVN1003 inhibits the in vitro phosphorylation of AKT and ERK 1/2 as well as either ibrutinib or idelalisib. MDVN1001 and MDVN1002 are potent single inhibitors of BTK and PI3Kδ, respectively, but these compounds only inhibited the phosphorylation of AKT or ERK 1/2 at the higher concentration of 1 μM. This could be due to the lower potency of MDVN1002 against PI3Kδ molecules or possibly due to a difference in the cell permeability of MDVN1001 and MDVN1002. Similar to the combo treatment with ibrutinib and idelalisib, combination treatment with MDVN1001 and MDVN1002 showed an additive effect on the inhibition of the phosphorylation of AKT and ERK1/2 upon BCR activation and on cell viability of DOHH-2 cells. Taken together, the data suggest a synergistic effect of dual inhibition of BTK and PI3Kδ and by MDVN1003. This is further supported by the superior efficacy of MDVN1003 in the xenograft model as compared with either ibrutinib or idelalisib dosed individually. The difference in potency of MDVN1003 against BTK and PI3Kδ could explain why treatment with this compound is not as effective as combo dosing of ibrutinib and idelalisib in vitro or in vivo (Figs. 4 and 6). Further investigation of the structure-activity relationships of these compounds would be required to identify more potent dual BTK and PI3Kδ inhibitors with good oral bioavailability that could be tested for better efficacy in vivo.

Another possibility for the superior performance of MDVN1003 compared with monotherapy in the tumor xenograft model is that the antitumor effect could be unrelated to the inhibition of BTK or PI3Kδ. MDVN1003 inhibits many kinases at 1 μM (Fig. 3), so it is possible that the antitumor effect is not due to synergy of dual inhibition but instead due to the inhibition of another kinase that is required for the growth of DOHH-2 cells. Treatment with MDVN1001, MDV1002, or the combo treatment with these molecules was similarly as potent as MDVN1003 in the cell viability assay, which raises the possibility that the effect on cell viability by these three molecules may not be completely driven by the inhibition of BTK and PI3Kδ. However, MDVN1003 is not generally cytotoxic. This molecule, along with ibrutinib and idelalisib, did not induce cell death in HEL 92.1.7 erythroblasts (Fig. 4C). These cells do not express BTK or PI3Kδ, and any other kinase inhibited by MDVN1003 was not sufficient to induce cytotoxicity. Further optimization of the tool compound MDVN1003 is necessary to improve the selectivity profile and fully rule out off-target effects.

In practice, ibrutinib is extremely effective, and the 24-month progression-free survival in the phase I and phase II studies of ibrutinib in CLL was greater than 80% (Tucker and Rule, 2015). However, 30% of patients are initially refractory to ibrutinib (Tucker and Rule, 2015), and even more become resistant after long-term dosing (Byrd et al., 2013; Wang et al., 2013; Smith, 2015), so reducing the rate of resistance or increasing the duration of response could be important for treating patients with B cell malignancies. A potential advantage of combination therapy of BTK and PI3Kδ inhibitors may be to reduce the rate of acquired resistance to either BTK or PI3Kδ inhibition and potential efficacy in patients initially resistant to treatment of either a BTK or a PI3Kδ inhibitor. However, the preclinical data reported here and elsewhere (Jones and Byrd, 2014; Mathews Griner et al.,

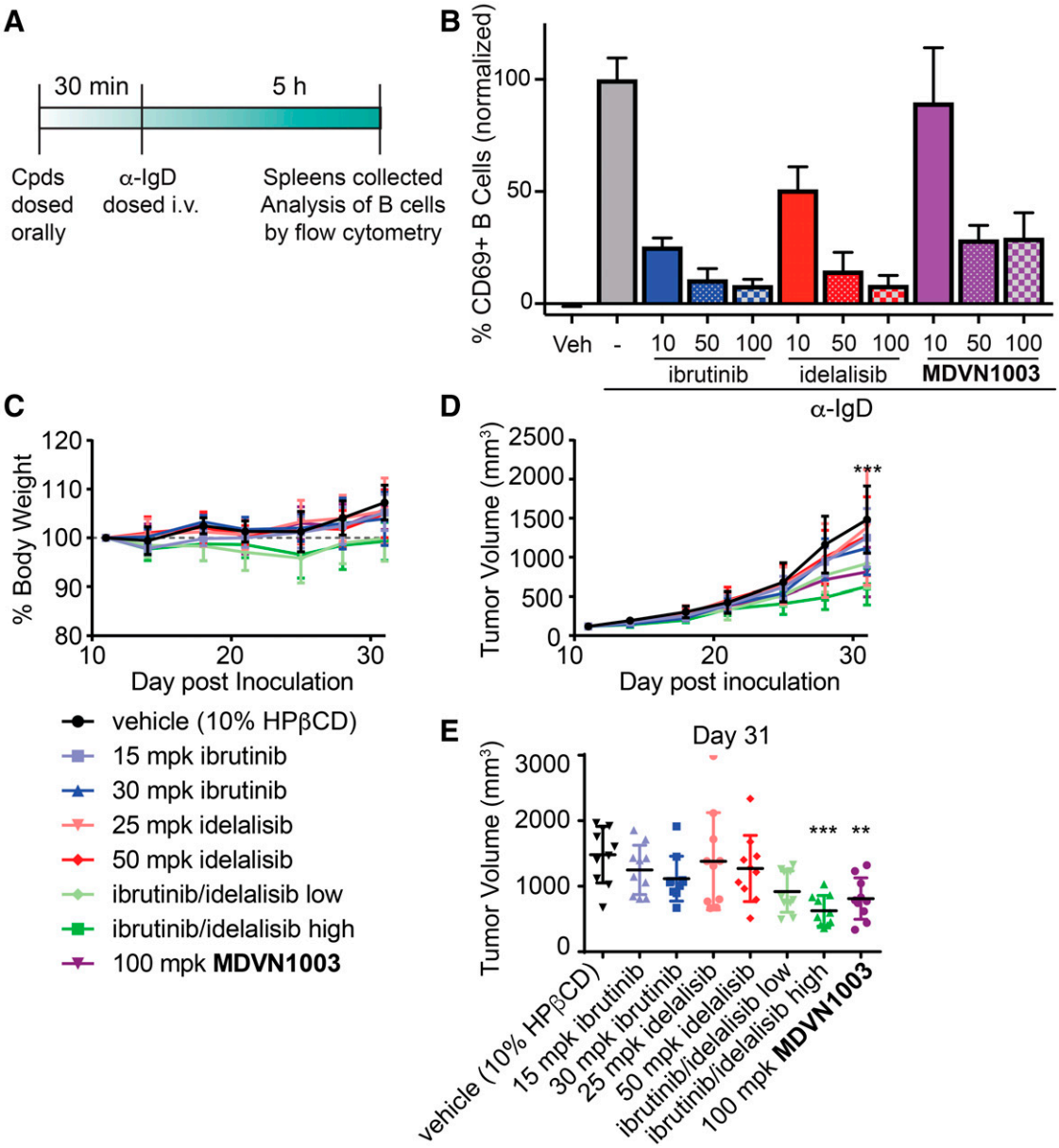

Fig. 6. MDVN1003 inhibits B cell activation in vivo and inhibits tumor growth in a B cell lymphoma xenograft model. (A) Scheme of the treatment conditions for the experiment in (B). (B) BALB/c mice were orally dosed with compounds or vehicle (Veh and -) at indicated concentrations for 30 minutes. Mice in all groups except the vehicle control were then dosed intravenously with α-IgD for 5 hours. Splenocytes were isolated and stained with a live/dead marker, αB220, and αCD69 antibodies. Activated B cells were determined as B220+CD69+ in a live gate by flow cytometry. Percentage of activated B cells post compound treatment was normalized to the percentage of active B cells in the α-IgD control (- in graph). (C–E) Compounds were tested in a mouse xenograft model of NHL. Ibrutinib was dosed at 15 mg/kg (light blue) or 30 mg/kg (dark blue); idelalisib was dosed at 25 mg/kg (pink) or 50 mg/kg (red); combo low dosing group was 15 mg/kg ibrutinib and 25 mg/kg idelalisib (ibrutinib/idelalisib low, light green); combo high dosing group was 30 mg/kg ibrutinib and 50 mg/kg idelalisib (ibrutinib/idelalisib high, dark green); MDVN1003 was dosed at 100 mg/kg. Ibrutinib was dosed orally once daily, and the other two compounds were dosed orally twice daily. (C) Average body weight of mice in each dosing group (mean ± standard deviation of $n = 10$ mice per group). (D) Average tumor volume of mice in each dosing group (mean ± standard deviation, $^{***}P < 0.001$, Kruskal-Wallis). (E) The tumor volume of each mouse in the dosing groups on the final day of dosing (day 31 post inoculation). The black line is the average tumor volume of each group, and the colored lines are the standard deviations ($^{***}P < 0.001$, $^{**}P < 0.01$, Kruskal-Wallis corrected for multiple comparisons). Cpds, Compounds; HPβCD, hydroxypropyl beta-Cyclodextrin; mpk, mg/kg.

2014; Zhang et al., 2014; de Rooij et al., 2015; Koehrer and Burger, 2016) do not directly test whether dual inhibition or codosing is efficacious in the case of resistance. To date, no preclinical or clinical studies have looked at the effects of cotreatment with BTK and PI3Kδ inhibitors on the rates of resistance. In fact, there is a dearth of reagents with which to investigate these questions and a lack of knowledge around adaptive resistance to PI3Kδ inhibition.

In summary, our results show that dual inhibition of BTK and PI3Kδ by treatment with a single dual inhibitor could potentially improve the outcomes of NHL patients and may prevent resistance or extend the duration of response. Although MDVN1003 proved useful as an initial tool compound, further medicinal chemistry efforts are required to improve potency to achieve cytotoxic and tumor inhibitory effects that match the combination treatment with ibrutinib

and idelalisib. Additional investigation is required to better understand the mechanisms by which resistance to ibrutinib and idelalisib occurs and generate reagents to better elucidate preclinical efficacy. The results presented here provide a proof of concept that a dual inhibitor of BTK and PI3Kδ in a single molecule can be developed and could be used as a viable approach for the treatment of B cell malignancies.

Acknowledgments

The authors thank Katherine Stack from Fundación Ciencia y Vida for help with animal studies, and Ashu Gupta and the bioanalytical group at Integral BioSciences for the execution of key in vitro metabolism studies that produced important steps forward in the program. The authors acknowledge the skilled researchers at Reaction Biology and Crown Biosciences for their work.

Authorship Contributions

Participated in research design: McCullagh, Alfaro, Bernales, Quinn, Hung.

Conducted experiments: Alfaro, Pérez de Arce, Avila, Gaete, Fuentealba, Kanno, Almirez, Flores, Belmar, Ureta, Delgado, Acuña.

Contributed new reagents or analytic tools: Pham, Pujala, Barde, Nayak, Upendra, Patel, Chauhan, Sharma, Rai, Chakravarty.

Performed data analysis: McCullagh, Alfaro, Quinn, Perez de Arce, Gaete, Fuentealba, Flores, Belmar, Ureta.

Wrote or contributed to the writing of the manuscript: McCullagh, Alfaro, Pham, Rai, Quinn.

References

Berndt A, Miller S, Williams O, Le DD, Houseman BT, Pacold JI, Gorrec F, Hon WC, Liu Y, Rommel C, et al. (2010) The p110 delta structure: mechanisms for selectivity and potency of new PI(3)K inhibitors. *Nat Chem Biol* **6**:117–124.

Buchner M and Müschen M (2014) Targeting the B-cell receptor signaling pathway in B lymphoid malignancies. *Curr Opin Hematol* **21**:341–349.

Byrd JC, Furman RR, Coutre SE, Flinn IW, Burger JA, Blum KA, Grant B, Sharman JP, Coleman M, Wierda WG, et al. (2013) Targeting BTK with ibrutinib in relapsed chronic lymphocytic leukemia. *N Engl J Med* **369**:32–42.

Davids MS, Kim HT, Nicotra A, Saveli A, Francoeur K, Hellman JM, Miskin H, Sportelli P, Rado T, Bashey A, et al. (2016) Preliminary Results of a Phase I/Ib Study of Ibrutinib in Combination with TGR-1202 in Patients with Relapsed/Refractory CLL or MCL, in *2016 Annual Congress of the European Hematology Association*, Copenhagen, Denmark.

Davies B and Morris T (1993) Physiological parameters in laboratory animals and humans. *Pharm Res* **10**:1093–1095.

de Rooij MF, Kuil A, Kater AP, Kersten MJ, Pals ST, and Spaargaren M (2015) Ibrutinib and idelalisib synergistically target BCR-controlled adhesion in MCL and CLL: a rationale for combination therapy. *Blood* **125**:2306–2309.

Do B, Mace M, and Rexwinkle A (2016) Idelalisib for treatment of B-cell malignancies. *Am J Health Syst Pharm* **73**:547–555.

Fruman DA and Rommel C (2014) PI3K and cancer: lessons, challenges and opportunities. *Nat Rev Drug Discov* **13**:140–156.

Honigberg LA, Smith AM, Chen J, Thiemann P, and Verner E(2007) Targeting Btk in lymphoma: PCI-32765 inhibits tumor growth in mouse lymphoma models and a fluorescent analog of PCI-32765 is an active-site probe that enables assessment of Btk inhibition in vivo. *Blood* **110**:1592.

Honigberg LA, Smith AM, Sirisawad M, Verner E, Loury D, Chang B, Li S, Pan Z, Thamm DH, Miller RA, et al. (2010) The Bruton tyrosine kinase inhibitor PCI-32765 blocks B-cell activation and is efficacious in models of autoimmune disease and B-cell malignancy. *Proc Natl Acad Sci USA* **107**:13075–13080.

Howlader NNA, Krapcho M, Garshell J, Miller D, Altekruse SF, Kosary CL, Yu M, Ruhl J, Tatalovich Z, Mariotto A et al. (eds) (2014) SEER Cancer Statistics Review, 1975–2011, National Cancer Institute. Bethesda, MD, http://seer.cancer.gov/csr/1975_2011/.

Jones JA and Byrd JC (2014) How will B-cell-receptor-targeted therapies change future CLL therapy? *Blood* **123**:1455–1460.

Koehrer S and Burger JA (2016) B-cell receptor signaling in chronic lymphocytic leukemia and other B-cell malignancies. *Clin Adv Hematol Oncol* **14**:55–65.

Lannutti BJ, Meadows SA, Herman SE, Kashishian A, Steiner B, Johnson AJ, Byrd JC, Tyner JW, Loriaux MM, Deininger M, et al. (2011) CAL-101, a p110delta selective phosphatidylinositol-3-kinase inhibitor for the treatment of B-cell malignancies, inhibits PI3K signaling and cellular viability. *Blood* **117**:591–594.

Marcotte DJ, Liu YT, Arduini RM, Hession CA, Miatkowski K, Wildes CP, Cullen PF, Hong V, Hopkins BT, Mertsching E, et al. (2010) Structures of human Bruton's tyrosine kinase in active and inactive conformations suggest a mechanism of activation for TEC family kinases. *Protein Sci* **19**:429–439.

Marini BL, Samanas L, and Perissinotti AJ (2016) Expanding the armamentarium for chronic lymphocytic leukemia: a review of novel agents in the management of chronic lymphocytic leukemia. *J Oncol Pharm Pract* 1078155216656929 [published ahead of print].

Mathews Griner LA, Guha R, Shinn P, Young RM, Keller JM, Liu D, Goldlust IS, Yasgar A, McKnight C, Boxer MB, et al. (2014) High-throughput combinatorial screening identifies drugs that cooperate with ibrutinib to kill activated B-cell-like diffuse large B-cell lymphoma cells. *Proc Natl Acad Sci USA* **111**:2349–2354.

Pan Z, Scheerens H, Li SJ, Schultz BE, Sprengeler PA, Burrill LC, Mendonca RV, Sweeney MD, Scott KC, Grothaus PG, et al. (2007) Discovery of selective irreversible inhibitors for Bruton's tyrosine kinase. *ChemMedChem* **2**:58–61.

Pujala B, Agarwal AK, Middya S, Banerjee M, Surya A, Nayak AK, Gupta A, Khare S, Guguloth R, Randive NA, et al. (2016) Discovery of Pyrazolopyrimidine Derivatives as Novel Dual Inhibitors of BTK and PI3Kδ. *ACS Med Chem Lett* **7**:1161–1166.

Puri KD, Di Paolo JA, and Gold MR (2013) B-cell receptor signaling inhibitors for treatment of autoimmune inflammatory diseases and B-cell malignancies. *Int Rev Immunol* **32**:397–427.

Qu F-L, Xia B, Li S-X, Tian C, Yang H-L, Li Q, Wang Y-F, Yu Y, and Zhang Y-Z (2015) Synergistic suppression of the PI3K inhibitor CAL-101 with bortezomib on mantle cell lymphoma growth. *Cancer Biol Med* **12**:401–408.

Sancho D, Gómez M, and Sánchez-Madrid F (2005) CD69 is an immunoregulatory molecule induced following activation. *Trends Immunol* **26**:136–140.

Seda V and Mraz M (2015) B-cell receptor signalling and its crosstalk with other pathways in normal and malignant cells. *Eur J Haematol* **94**:193–205.

Shanafelt TD, Borah BJ, Finnes HD, Chaffee KG, Ding W, Leis JF, Chanan-Khan AA, Parikh SA, Slager SL, Kay NE, et al. (2015) Impact of ibrutinib and idelalisib on the pharmaceutical cost of treating chronic lymphocytic leukemia at the individual and societal levels. *J Oncol Pract* **11**:252–258.

Smith MR (2015) Ibrutinib in B lymphoid malignancies. *Expert Opin Pharmacother* **16**:1879–1887.

Swerdlow SH, Campo E, Pileri SA, Harris NL, Stein H, Siebert R, Advani R, Ghielmini M, Salles GA, Zelenetz AD, et al. (2016) The 2016 revision of the World Health Organization classification of lymphoid neoplasms. *Blood* **127**:2375–2390.

Tomlinson MG, Woods DB, McMahon M, Wahl MI, Witte ON, Kurosaki T, Bolen JB, and Johnston JA (2001) A conditional form of Bruton's tyrosine kinase is sufficient to activate multiple downstream signaling pathways via PLC Gamma 2 in B cells. *BMC Immunol* **2**:4.

Tucker DL and Rule SA (2015) A critical appraisal of ibrutinib in the treatment of mantle cell lymphoma and chronic lymphocytic leukemia. *Ther Clin Risk Manag* **11**:979–990.

Verkoczy L, Duong B, Skog P, Aït-Azzouzene D, Puri K, Vela JL, and Nemazee D (2007) Basal B cell receptor-directed phosphatidylinositol 3-kinase signaling turns off RAGs and promotes B cell-positive selection. *J Immunol* **178**:6332–6341.

Wang ML, Rule S, Martin P, Goy A, Auer R, Kahl BS, Jurczak W, Advani RH, Romaguera JE, Williams ME, et al. (2013) Targeting BTK with ibrutinib in relapsed or refractory mantle-cell lymphoma. *N Engl J Med* **369**:507–516.

Woyach JA, Johnson AJ, and Byrd JC (2012) The B-cell receptor signaling pathway as a therapeutic target in CLL. *Blood* **120**:1175–1184.

Zhang Q, Xia B, Qu F, Yuan T, Guo S, Zhao W, Li Q, Yang H, Wang Y, and Zhang Y (2014) [Effect of PI3Kδ inhibitor CAL-101 on myeloma cell lines and preliminary study of synergistic effects with other new drugs]. *Zhonghua Xue Ye Xue Za Zhi* **35**:926–930.

Address correspondence to: Emma McCullagh, 525 Market Street, 36th Floor, San Francisco, CA 94105. E-mail: Emmamccullagh@yahoo.com

Dual Inhibition of Bruton's Tyrosine Kinase and Phosphoinositide-3-Kinase p110δ as a Therapeutic Approach to Treat Non-Hodgkin's B cell Malignancies

Jennifer Alfaro[1], Felipe Pérez de Arce, Sebastián Belmar, Glenda Fuentealba, Patricio Avila, Gonzalo Ureta, Camila Flores, Claudia Acuña, Luz Delgado, Diana Gaete, Brahmam Pujala, Anup Barde, Anjan K. Nayak, TVR Upendra, Dhananjay Patel, Shailender Chauhan, Vijay K. Sharma, Stacy Kanno, Ramona G. Almirez, David T. Hung, Sarvajit Chakravarty, Roopa Rai, Sebastián Bernales, Kevin P. Quinn, Son M. Pham, Emma McCullagh[1]

Translational Research Group, Fundación Ciencia y Vida *(J.A., F.P., S.B., G.F., P.A., G.U., C.F., C.A., L.D., D.A.)*
Biological Sciences Department, Facultad de Ciencias Biológicas, Universidad Andrés Bello *(F.P., S.B.)*
Chemistry Group, Integral BioSciences, Pvt. Ltd. *(B.P., A.B., A.K.N, TVR.U., D.P, S.C., V.K.S.)*
Discovery Research, Medivation, Inc. now Pfizer *(S.K., R.G.A, D.T.H., S.C., R.R., S.B., K.P.Q., S.M.P., E.M.)*

Journal of Pharmacology and Experimental Therapeutics

SUPPLEMENTARY INFORMATION

Table of Contents **Page**

Supplementary Figure 1

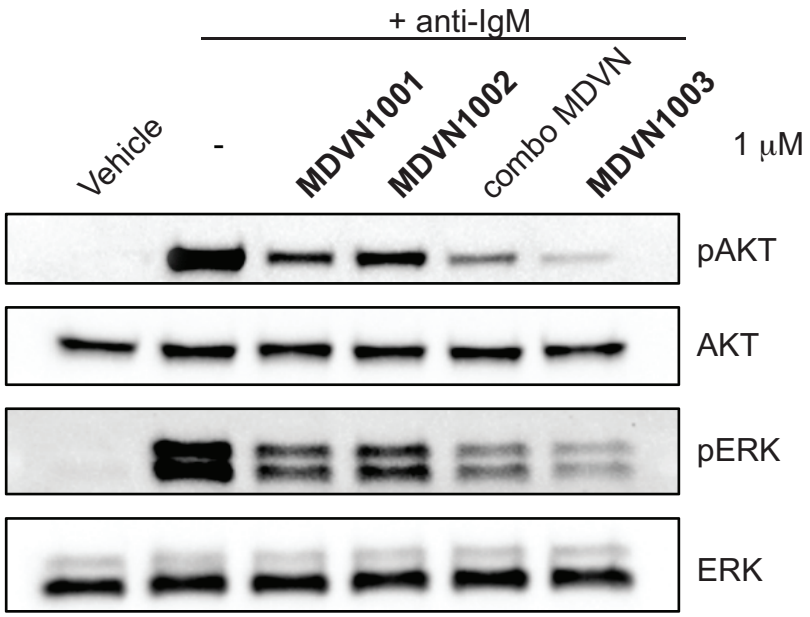

Supplementary Figure 1: BTK and PI3Kδ inhibitor compounds differentially inhibit the phosphorylation of downstream signaling molecules ATK and ERK. Ramos cell were pretreated with 1 μM of the indicated compounds or DMSO (vehicle and -) for 30 min. All samples except for the vehicle control were treated with α-IgM (1.3 μg/ml) for 5 min to activate BCR signaling. Levels of pAKT and pERK 1/2 and the corresponding total proteins were determined by western blot. Combo is equimolar (1 μM) treatment of ibrutinib and idelalisib and combo MDVN is equimolar (1 μM) treatment of **MDVN1001** and **MDVN1002**.

Supplementary Figure 2

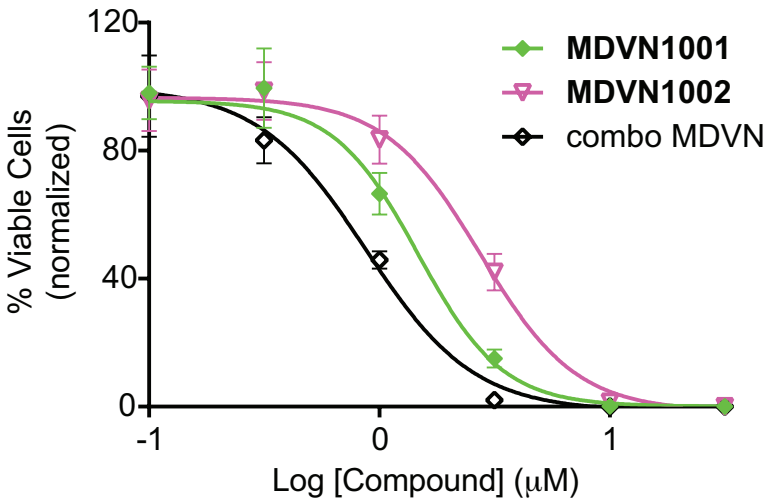

Compound	IC50 (μM)
MDVN1001	1.47
MDVN1002	2.75
combo MDVN	0.87

Supplementary Figure 2: Combination treatment of **MDVN1001** and **MDVN1002** on cell viability of DOHH-2 cells. DOHH-2 cells were treated with **MDVN1001** or **MDVN1002** or equimolar concentrations of both compounds for 72 h. Cell viability was measured as described in the Materials and Methods. The IC_{50} was calculated from the curve fitted to the data points by non-linear regression using GraphPad Prism.

General Synthesis Information

^{1}H NMR spectra and ^{13}C NMR spectra were recorded on a Varian 400 MHz spectrometer. Spectra are referenced to residual chloroform (δ 7.26, ^{1}H), DMSO (δ 2.54, ^{1}H) or methanol (δ 3.34, ^{1}H) unless otherwise noted. Chemical shifts are reported in ppm (δ); multiplicities are indicated by s (singlet), d (doublet), t (triplet), q (quartet), quint (quintet), sext (sextet), m (multiplet) and br (broad). Coupling constants, *J*, are reported in Hertz. Silica gel chromatography was performed using a Teledyne Isco CombiFlash® Rf+ instrument using Hi-Purit Silica Flash Cartridges (National Chromatography Inco) or RediSep Rf Gold C18 Cartridges (Teledyne Isco). Analytical HPLC was performed on a Waters ACQUITY UPLC with a photodiode array detector using and a Waters ACQUITY BEH Shield RPC18 (2.1 × 50 mm, 1.7 μm) column. Analytical LCMS was performed on a Waters ACQUITY UPLC with a Waters 3100 mass detector. Chiral HPLC was performed on a Waters Alliance e2695 with a photodiode array detector using Daicel Chiralpak® AD-H, Chiralpak® IA, Chiralpak® IB, Chiralpak® IC, Chiralcel® OD-H or Chiralcel® OJ-H columns. Optical rotations were obtained on a Jasco P-2000 digital polarimeter and are reported as $[\alpha]_D^T$ temperature (T), concentration (*c* = g/100 mL) and solvent. Commercially available reagents and solvents were used as received unless otherwise indicated.

Literature Preparations

The following compounds were prepared by literature methods: 5-bromo-2,3-dihydro-1*H*-inden-2-ol (**I**)[Ref: Goeksu *et al.* Tetrahedron, 61(28), 6801-6807; 2005], 3-iodo-1*H*-pyrazolo[3,4-*d*]pyrimidin-4-amine (**V**)[Ref: Rai *et al.* PCT Application WO2015/058084 A1, 2015], 1-(5-amino-2,3-dihydro-1*H*-inden-2-yl)-3-(8-fluoro-3,4-dihydro-2*H*-benzo[*b*][1,4]oxazin-6-yl)-1*H*-pyrazolo[3,4-*d*]pyrimidin-4-amine (**MDVN1003**).[1]

General Scheme for the Preparation of MDVN1001

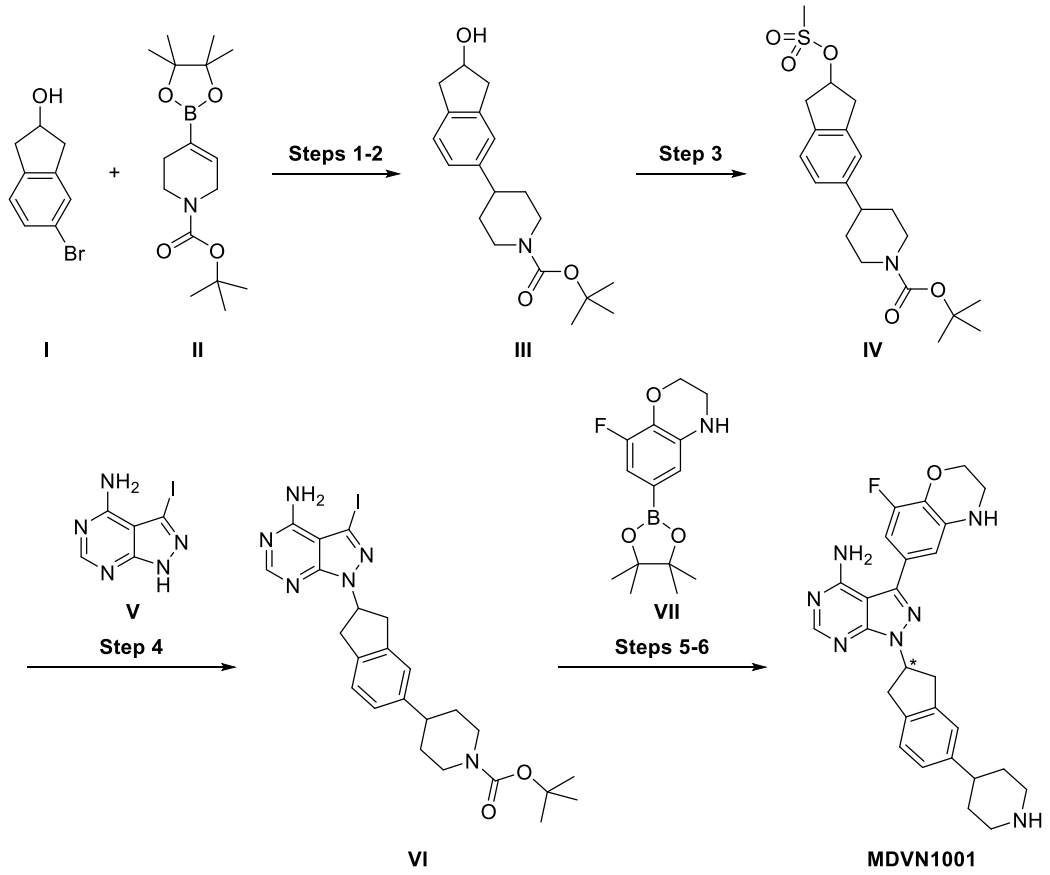

Preparation of *tert*-butyl 4-(2-hydroxy-2,3-dihydro-1*H*-inden-5-yl)piperidine-1-carboxylate (III)

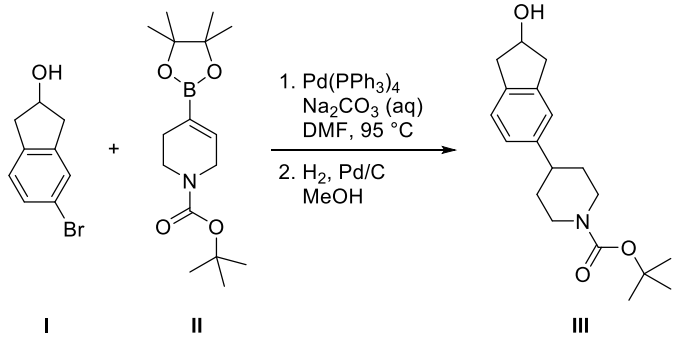

Step 1. To a stirred solution of **I** (1 g, 4.72 mmol) in DMF (14 mL) was added **II** (2.17 g, 7.03 mmol, 1.5 eq), $Pd(PPh_3)_4$ (380 mg, 0.33 mmol, 0.07 eq) and Na_2CO_3 (1.5 g, 14.2 mmol, 3 eq) as a solution in water (14 mL). The reaction was heat to 95 °C and stirred for 2 h. Upon completion, the mixture was extracted with EtOAc (200 mL × 3). The combined organic layers were washed with water (30 mL × 3), dried over anhydrous Na_2SO_4, filtered and concentrated *in vacuo* to afford *tert*-butyl 4-(2-hydroxy-2,3-dihydro-1*H*-

inden-5-yl)-3,6-dihydropyridine-1(2*H*)-carboxylate (900 mg, 60%). The material was used without further purification.

Analytical data

LC-MS 315 $[M+H]^+$

Step 2. A round-bottom flask was charged with *tert*-butyl 4-(2-hydroxy-2,3-dihydro-1*H*-inden-5-yl)-3,6-dihydropyridine-1(2*H*)-carboxylate (900 mg, 2.86 mmol), Pd/C (10 wt. %, 200 mg) and MeOH (50 mL). The flask was then charged with H_2 gas (1 atm). The reaction mixture was allowed to stir overnight at room temperature. Upon completion, the contents were filtered through a bed of Celite® and washed with MeOH (30 mL × 3). Residual Pd/C was carefully quenched with aqueous HCl. The supernatant was then concentrated *in vacuo* to afford **III** (900 mg, 99%) which was used without further purification.

Analytical data

^{1}H NMR (400 MHz, CD_3OD) δ 7.71-7.58 (m, 2H), 7.58-7.51 (m, 1H), 4.60 (s, 1H), 4.19 (d, J = 13.2 Hz, 2H), 3.16-3.06 (m, 2H), 2.91-2.77 (m, 4H), 2.70-2.60 (m, 1H), 1.78 (d, J = 12.7 Hz, 2H), 1.58 (d, J = 3.9 Hz, 2H), 1.51-1.41 (m, 9H).

Preparation of *tert*-butyl 4-(2-((methylsulfonyl)oxy)-2,3-dihydro-1*H*-inden-5-yl)piperidine-1-carboxylate (IV)

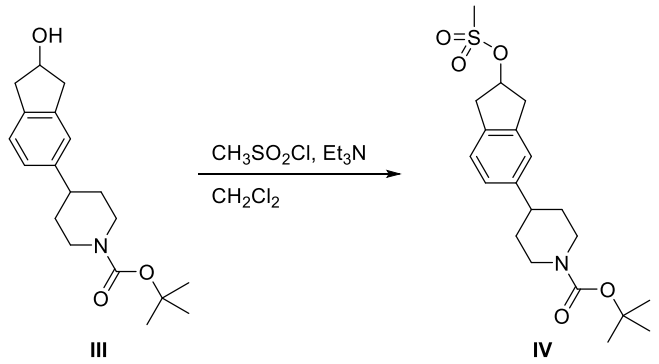

Step 3. To a solution of **III** (900 mg, 2.84 mmol) in CH_2Cl_2 (30 mL) was added Et_3N (1.43 g, 14.2 mmol, 5 eq). The mixture was cooled to 0 °C and methanesulfonyl chloride (638 mg, 5.68 mmol, 2 eq) was slowly added dropwise. The mixture was warmed to room temperature and allowed to stir for 2 h. Upon completion the reaction mixture was extracted with EtOAc (200 mL × 3). The combined organic layers were washed with water (100 mL × 3) followed by brine (30 mL × 2). The organic layer was dried over anhydrous Na_2SO_4, filtered and concentrated *in vacuo* to afford **IV** (1.1 g, 98%) which was used without further purification.

Analytical data

^{1}H NMR (400 MHz, CD_3OD) δ 7.66 (d, *J* = 7.0 Hz, 1H), 7.69 (d, *J* = 7.4 Hz, 1H), 7.48 (d, *J* = 7.8 Hz, 1H), 5.52 (br s, 1H), 3.33 (d, *J* = 4.7 Hz, 2H), 3.24 (br s, 2H), 3.15 (m, 2H), (3.03 (d, *J* = 2.0 Hz, 3H), 2.79 (br s, 2H), 2.70-2.59 (m, 1H), 1.80 (d, *J* = 12.9 Hz, 2H), 1.67-1.59 (m, 2H), 1.50-1.44 (m, 9H).

Preparation of *tert*-butyl 4-(2-(4-amino-3-iodo-1*H*-pyrazolo[3,4-*d*]pyrimidin-1-yl)-2,3-dihydro-1*H*-inden-5-yl)piperidine-1-carboxylate (VI)

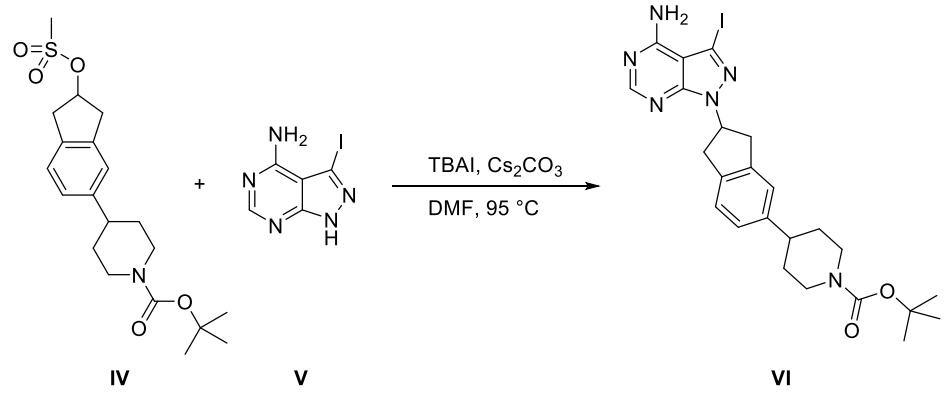

IV V VI

Step 4. Cs_2CO_3 (1 g, 3.08 mmol, 2 eq) was added to a suspension of **V** (400 mg, 1.54 mmol) in DMF (10 mL). The reaction mixture was allowed to stir for 45 min at room temperature. Intermediate **IV** (1.1 g, 2.77 mmol, 1.8 eq) and tetrabutylammonium iodide (104 mg, 0.31 mmol, 0.2 eq) were then added. The mixture was then heated to 95 °C and allowed to stir for 3 h. Upon completion, the mixture was allowed to cool and water (50 mL) was added. The resulting precipitate was collected by vacuum filtration. The filter cake was carefully washed with cold water (40 mL × 2) followed by cold *n*-pentane (40 mL × 3). The solids were dried under reduced pressure to afford **VI** (350 mg, 41%) which was used without further purification.

Analytical data

LC-MS 561$[M+H]^+$

Preparation of 3-(8-fluoro-3,4-dihydro-2*H*-benzo[*b*][1,4]oxazin-6-yl)-1-(5-(piperidin-4-yl)-2,3-dihydro-1*H*-inden-2-yl)-1*H-pyrazolo*[3,4-*d*]pyrimidin-4-amine (MDVN1001)

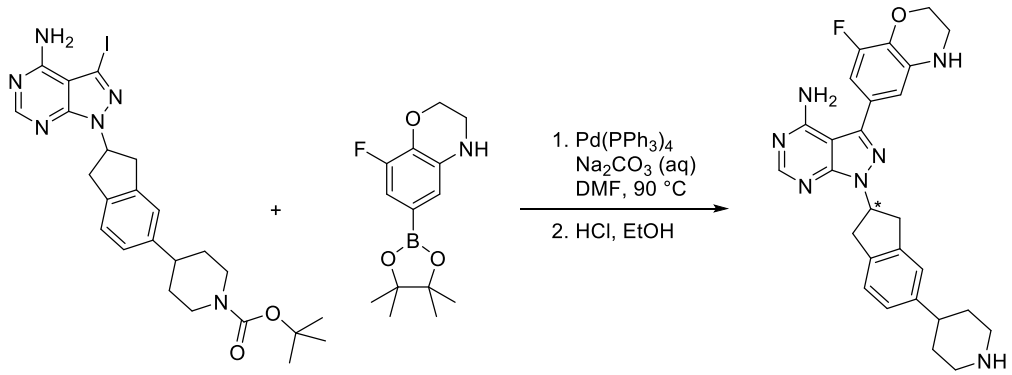

VI VII MDVN1001

Step 5. A reaction vessel was charged with **VI** (350 mg, 0.625 mmol) and DMF (5 mL). To this was added **VII** (261 mg, 0.938 mmol, 1.5 eq), $Pd(PPh_3)_4$ (58 mg, 0.05 mmol, 0.08 eq) and Na_2CO_3 (199 mg, 1.88 mmol, 3 eq) as a solution in water (5 mL). The reaction mixture was heated to 90 °C with stirring and allowed to progress for 3 h. Upon completion, the reaction was quenched with ice cold water (30 mL). The resulting precipitate was collected by vacuum filtration. The filter cake was washed with cold water (40 mL × 3) and cold *n*-pentane (30 mL × 3). The solids were dried under reduced pressure to afford a crude product which was purified by reversed-phase SiO_2 chromatography (55% CH_3CN in 10 mM NH_4OAc). The enantiomers were then separated by chiral preparative HPLC to afford *tert*-butyl 4-(2-(4-amino-3-(8-fluoro-3,4-dihydro-2*H*-benzo [*b*][1,4] oxazin-6-yl)-1*H*-pyrazolo[3,4-*d*]pyrimidin-1-yl)-2,3-dihydro-1*H*-inden-5-yl)piperidine-1-carboxylate (12 mg, 3%) as a single enantiomer.

Analytical data

LC-MS 586 $[M+H]^+$

Step 6. To a reaction vessel containing *tert*-butyl 4-(2-(4-amino-3-(8-fluoro-3,4-dihydro-2*H*-benzo[*b*][1,4]oxazin-6-yl)-1*H*-pyrazolo[3,4-*d*]pyrimidin-1-yl)-2,3-dihydro-1*H*-inden-5-yl)piperidine-1-carboxylate (12 mg, 0.02 mmol) was added ethanolic HCl (4 mL) and the resulting mixture was allowed to stir overnight at room temperature. Upon completion, the reaction mixture was concentrated and lyophilized to afford **MDVN1001** as a single enantiomer and hydrochloride salt (6 mg, 57%).

Analytical data

LC-MS 486 $[M+H]^+$

^{1}H NMR (400 MHz, CD_3OD) δ 8.33 (s, 1H), 7.29 (d, J = 7.8 Hz, 1H), 7.26-7.13 (m, 3H), 6.44 (d, J = 6.1 Hz, 2H), 5.76 (d, J = 6.2 Hz, 1H), 4.25 (t, J = 4.3 Hz, 2H), 3.63-3.46 (m, 6H), 3.39 (dd, J = 25.4, 5.1 Hz, 6H), 3.14 (s, 2H), 2.92 (s, 1H), 2.09 (d, J = 14.2 Hz, 2H), 1.93 (t, J = 12.9 Hz, 2H).

General Scheme for the Preparation of MDVN1002

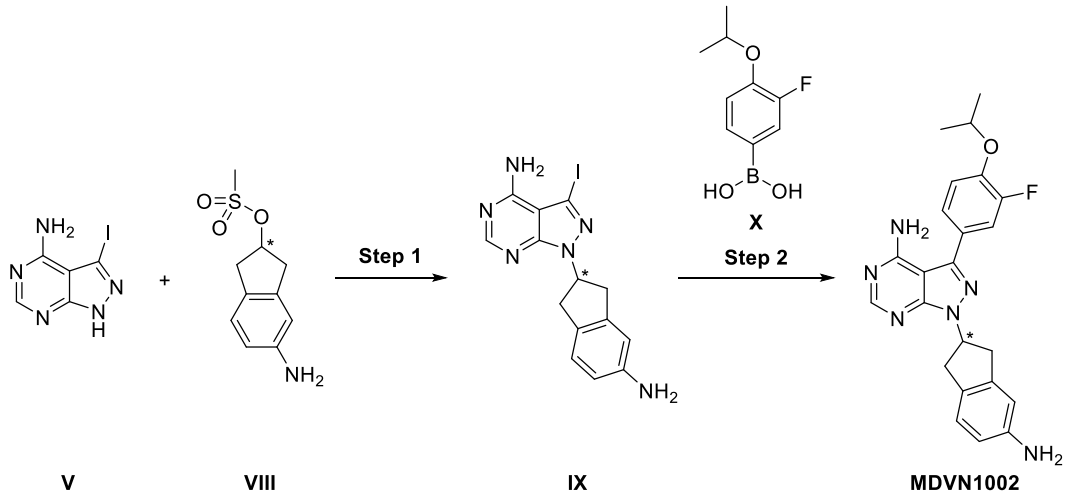

Preparation of 1-(5-amino-2,3-dihydro-1*H*-inden-2-yl)-3-iodo-1*H*-pyrazolo[3,4-*d*]pyrimidin-4-amine (IX)

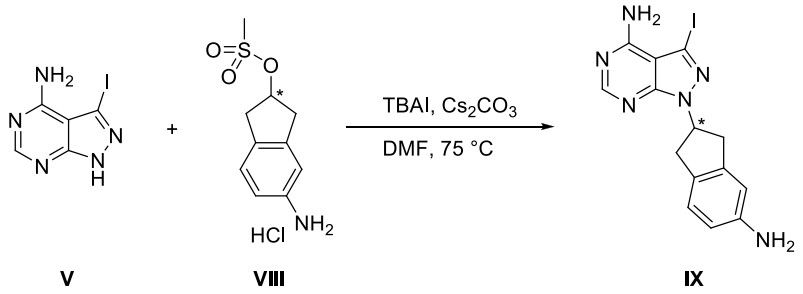

Step 1. Cs_2CO_3 (3.49 g, 10.7 mmol, 2 eq) was added to a stirred suspension of **V** (1.4 g, 5.36 mmol) in DMF (15 mL) at room temperature. The reaction mixture was allowed to stir for 45 min at room temperature. Intermediate **VIII** (1.82 g, 8.04 mmol, 1.5 eq) and tetrabutylammonium iodide (396 mg, 0.107 mmol, 0.02 eq) were then added. The mixture was then heated to 75 °C and allowed to stir for 90 min. Upon completion, the mixture was allowed to cool and water (30 mL) was added. The resulting precipitate was collected by vacuum filtration. The filter cake was triturated with hexane (10 mL × 2). The solids were dried under reduced pressure to afford **IX** (1.7 g, 81%) which was used without further purification.

Analytical data

LC-MS 393 $[M+H]^+$

Preparation of 1-(5-amino-2,3-dihydro-1*H*-inden-2-yl)-3-(3-fluoro-4-isopropoxyphenyl)-1*H*-pyrazolo[3,4-*d*]pyrimidin-4-amine (MDVN1002)

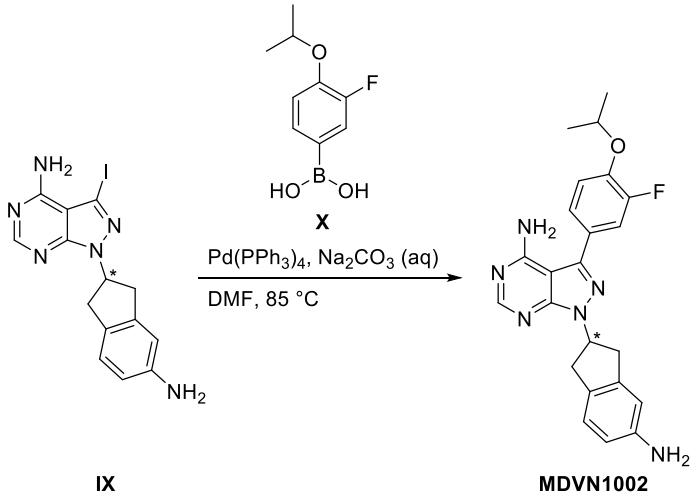

Step 2. A reaction vessel was charged with **IX** (200 mg, 0.51 mmol) and DMF (3 mL). To this was added **X** (152 mg, 0.77 mmol, 1.5 eq), $Pd(PPh_3)_4$ (41 mg, 0.036 mmol, 0.07 eq) and Na_2CO_3 (162 mg, 1.53 mmol, 3 eq) as a solution in water (3 mL). The reaction mixture was heated to 85 °C with stirring and allowed to progress overnight. Upon completion, the reaction was quenched with ice cold water (50 mL). The resulting precipitate was collected by vacuum filtration. The filter cake was washed with cold water (30 mL × 2) and cold *n*-pentane (40 mL × 2). The solids were dried under reduced pressure to afford a crude product which was purified by reversed-phase SiO_2 chromatography (55-60% CH_3CN in 10 mM NH_4OAc) to afford **MDVN1002** as a single enantiomer (90 mg, 42%).

Analytical data

LC-MS 419 $[M+H]^+$

^{1}H NMR (400 MHz, CD_3OD) δ 8.25 (s, 1H), 7.85 (s, 1H), 7.46–7.37 (m, 2H), 7.23 (t, *J* = 8.6 Hz, 1H), 6.99 (d, *J* = 8.0 Hz, 1H), 6.69–6.58 (m, 1H), 5.69 (q, *J* = 8.3 Hz, 1H), 4.79 (s, 1H), 4.69 (p, *J* = 6.1 Hz, 1H), 3.50 (ddd, *J* = 30.0, 15.5, 8.2 Hz, 2H), 3.35 (d, *J* = 5.7 Hz, 1H), 1.38 (d, *J* = 6.1 Hz, 6H).

General Scheme for the Preparation of Intermediate VIII

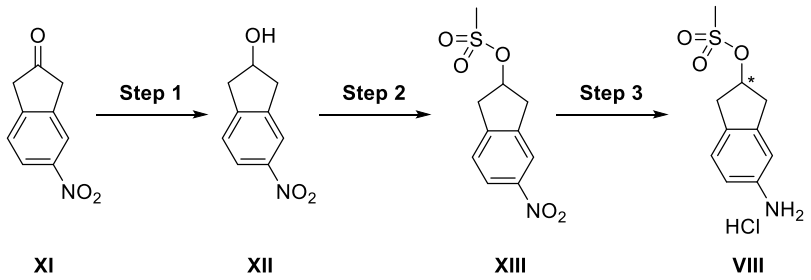

Preparation of 5-nitro-2,3-dihydro-1*H*-inden-2-ol (XII)

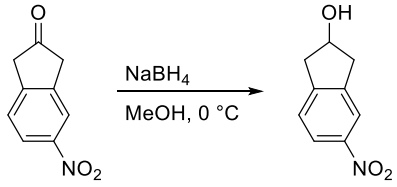

Step 1. To the stirred solution of **XI** (50 g, 0.282 mol) in MeOH (2 L) was added $NaBH_4$ (21.5 g, 0.565 mol, 2 eq) at 0 °C portion wise. The reaction mixture was allowed to stir at 0 °C for 1 h. The reaction was monitored by TLC. Upon completion, the reaction mixture was concentrated under reduced pressure. The residue was treated with CH_2Cl_2, filtered and washed with additional CH_2Cl_2. The filtrate was concentrated *in vacuo* to afford **XII** (43 g, 85%) as light brown solid. The material was used without further purification.

Analytical data

LC-MS 180 $[M+H]^+$

Preparation of 5-nitro-2,3-dihydro-1*H*-inden-2-yl methanesulfonate (XIII)

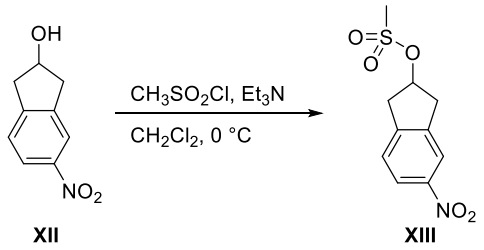

XII **XIII**

Step 2. To the stirred solution of **XII** (81 g, 0.45 mol) in CH_2Cl_2 (2.5 L) was added Et_3N (206 g, 2.00 mol, 4.4 eq) at 0 °C followed by the slow addition of methanesulfonyl chloride (104 g, 0.91 mol, 2 eq). The reaction was allowed to stir at 0 °C for 1.5 h. Upon completion, the reaction mixture was diluted with water and extracted with CH_2Cl_2. The organic layer was washed with brine, dried over anhydrous Na_2SO_4, filtered and concentrated *in vacuo*. The crude material was recrystallized with a mixture of CH_2Cl_2 and MTBE to afford **XIII** (92 g, 79%) as an off-white solid.

Analytical data

LC-MS 258 $[M+H]^+$

Preparation of (-)-5-amino-2,3-dihydro-1*H*-inden-2-yl methanesulfonate hydrochloride (VIII)

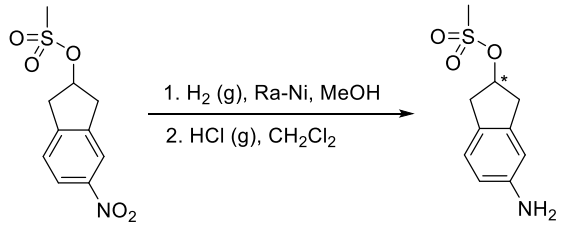

XIII **VIII**

Step 3. To the stirred solution of **XIII** (46 g, 0.179 mol) in MeOH (2 L) was added Raney-Ni (46 g, wet). The resulting reaction mixture was stirred for 3 h under H_2 (30 psi). The reaction mixture was filtered and the filter cake was washed with MeOH. The filtrate was concentrated *in vacuo* and treated with MTBE to afford (±)-5-amino-2,3-dihydro-1*H*-inden-2-yl methanesulfonate (28 g, 68%) as an off-white solid. The enantiomers were separated by chiral HPLC. The freebase was then diluted with CH_2Cl_2 and purged with HCl (g) at 0 °C for 3 h. The precipitate was filtered and washed with CH_2Cl_2 and MTBE to give **VIII** as a single enantiomer and hydrochloride salt. Peak 1HCl salt (batch 1, 10.8 g, 97.4% ee and batch 2 14.2 g, 98.9%ee) and peak 2 HCl salt (batch 1, 9.4 g, 97.7% ee and batch 2, 15.6 g, 98.4%ee) as an off-white solid.

Analytical data

LC-MS 228 $[M+H]^+$

^{1}H NMR (400 MHz, DMSO-d_6) δ 10.40 (br s, 2H), 7.39 (d, *J* = 8.0 Hz, 1H), 7.31 (s, 1H), 7.26–7.19 (m, 1H), 5.50 (m, 1H), 3.36 (m, 2H), 3.22 (s, 3H), 3.14 (m, 2H).

Pharmacokinetic Analysis

Intravenous and Oral Pharmacokinetics in Mice. Female BALB/c mice (age, 10–12 weeks; 18–20 g b.wt.) were used in the study. Food and water were given ad libitum. **MDVN1003** was administered intravenously, via the tail vein, at a dose of 2 mg/kg as a solution (1 mg/ml) in 20% DMSO, 40% PEG200 and 40% water at a dose volume of 2 ml/kg. The oral dose, 10 mg/kg, was administered by gavage at a dose volume of 10 ml/kg in 0.5% methylcellulose at a concentration of 1 mg/ml. At defined time points (5, 15 min, 30 min, and 1, 2, 4, 8, and 24 h after dose), groups of three mice per time point were sacrificed by an overdose of CO_2, and blood was collected by cardiac puncture and placed in tubes containing K_2EDTA as the anticoagulant. Plasma was obtained by centrifuging the blood samples at 800g for 10 min and storing at -60 to -80°C until analysis.

Intravenous and Oral Pharmacokinetics in Rats. Male Sprague-Dawley rats (age, 7–9 weeks; 250–300 g b.wt.) were used in the study. Three rats were used for the intravenous and oral studies each, in a parallel design. One day before the study, the jugular vein was cannulated in all the rats to be used. Rats were fasted overnight before dosing and fed 4 h after dose. Water was given ad libitum. **MDVN1003** (2 mg/kg) was administered intravenously as a bolus dose through the jugular vein, at a dose volume of 1 ml/kg (2 mg/ml) in saline. The oral dose (5 mg/kg) was administered by gavage at a dose volume of 5 mL/kg as a 1 mg/ml suspension in 0.5% methylcellulose in water. From each rat, serial blood samples (≈0.2 ml per sample) were drawn at 5 (IV only), 15, 30, and at 1, 2, 4, 6, 8, 12 and 24 h after dose and placed in tubes containing K_2EDTA as the anticoagulant. Plasma was obtained by centrifuging the blood samples at 1000g for 10 min and storing at -60 to 80°C until analysis.

Intravenous and Oral Pharmacokinetics in Dogs. Six male beagle dogs (age, 1–2 years; 9–11 kg b.wt.) were used in the study. Three dogs were used in the intravenous and oral studies each, in a parallel design. The dogs were fasted overnight before dose and fed 4 h after dose in the oral study. Water was given ad libitum. The intravenous dose (1 mg/kg) was given as a bolus (1 ml/kg) in 20% DMSO, 40% PEG200

and 40% water at a concentration of 1 mg/ml. The oral dose (3 mg/kg) was administered by gavage at a dose volume of 5 ml/kg as a suspension (0.6 mg/ml) in 0.5% methylcellulose in water. At defined time points (3 (IV only), 5 (IV only), 15, and 30 min and 1, 2, 4, 8, 12, 24, 26 and 48 h after dose), serial blood samples (≈1 ml) were collected from either the cephalic or jugular vein via a butterfly catheter and placed into a chilled polypropylene tube with K_2EDTA as the anticoagulant. Samples were centrifuged at 4°C at a speed of 1000g for 10 min, and plasma was harvested and stored at -60 to -80°C until analysis.

Sample Analysis. Plasma samples from mouse, rat, and dog (10-30 µL) were precipitated with of acetonitrile (200 µL) containing internal standard (warfarin) in a 96-well plate, vortexed for 5 min, and then centrifuged at 1500g for 10 min in a refrigerated centrifuge (Sorvall Legend X1R centrifuge, Thermo Scientific) at 4°C. Supernatants (100 µL) were transferred to a new 96-well plate containing 100 µL of 0.1% formic acid in each well. The plate was vortexed for approximately 10 minutes and then aliquots were injected for LC/MS/MS analysis. Sample analysis was carried out AB/MDS Sciex API 4000 LC/MS/MS System (Framingham, MA) interfaced with Shimadzu SIL-20AC HT autosampler and Prominence CBM-20A pumps (Kyoto, Japan). The mobile phase consisted of 0.1% formic acid in water (A) and 0.1% formic acid in acetonitrile (B). A ballistic gradient (5% B for 0.5 min then increased to 95% B in 1.5 min and hold for 1 min, then return to 5% B) was used to elute the analyte and internal standard with a Waters Atlantis T3 (3 µ, 2.1 x 50 mm, Milford, MA) at a flow rate of 0.6 ml/min. The ion-optics were optimize with Analyst software (v1.6) and **MDVN1003** was analyzed with multiple reaction monitoring experiment with the Q1 to Q3 transitions masses of m/z 418.1 – m/z 287.1, respectively. The internal standard, warfarin, was monitored with m/z 309.0 – m/z 163.0. The assay was linear between 1 and 5000 nM (dog plasma: lower limit of quantitation, 1 nM) and between 2.0 and 1000 nM (mouse and rat plasma: lower limit of quantitation, 2 and 3 nM, respectively). Criteria for accuracy and precision were met.

Pharmacokinetic Analysis. Noncompartmental PK parameters such as the total volume of distribution (V_d), systemic clearance (CL), elimination half-life ($t_{1/2}$), area under the plasma concentration-time curve up to the last nonzero concentration (AUC_{0-t}), area under the plasma concentration-time curve from time 0 to infinity ($AUC_{0-\infty}$), the time of maximum concentration in plasma (t_{max}), and the maximum concentration in plasma (C_{max}) were estimated Phoenix WinNonlin version 6.4 (Pharsight Corp, St Louis, MO). The terminal elimination rate constant was estimated from the terminal linear part of the log-linear plot (a minimum of three points on the linear phase). The linear trapezoidal method was used to compute the AUC. For rats and dogs, PK parameters were estimated in individual animals and averaged. For mice, the PK parameters were estimated using the mean concentration data. The absolute oral bioavailability, F (%), was calculated from, the dose normalized ratio of oral AUC to IV AUC.

[1] Pujala B, Agarwal AK, Middya S, Banerjee M, Surya A, Nayak AK, Gupta A, Khare S, Guguloth R, Randive NA, Shinde BU, Thakur A, Patel DI, Raja M, Green MJ, Alfaro J, Avila P, Pérez de Arce F, Almirez RG, Kanno S, Bernales S, Hung DT, Chakravarty S, McCullagh E, Quinn KP, Rai R and Pham SM (2016) Discovery of Pyrazolopyrimidine Derivatives as Novel Dual Inhibitors of BTK and PI3Kδ. *ACS Medicinal Chemistry Letters*.